THESIS

THREE REGIONAL CLIMATOLOGIES OF MARINE STRATOCUMULUS
CHARACTERISTICS USING THE A-TRAIN SATELLITE DATA

Submitted by

Jessica A. Ram

Department of Atmospheric Science

In partial fulfillment of the requirements

For the Degree of Master of Science

Colorado State University
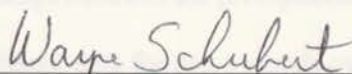
Fort Collins, Colorado
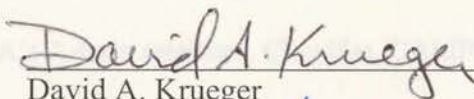
Summer 2010

COLORADO STATE UNIVERSITY

June 29, 2010

WE HEREBY RECOMMEND THAT THE THESIS PREPARED UNDER OUR SUPERVISION BY JESSICA A. RAM ENTITLED THREE REGIONAL CLIMATOLOGIES OF MARINE STRATOCUMULUS CHARACTERISTICS USING THE A-TRAIN SATELLITE DATA BE ACCEPTED AS FULFILLING IN PART REQUIREMENTS FOR THE DEGREE OF MASTER OF SCIENCE.
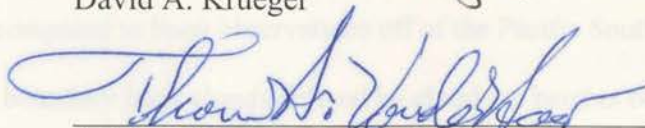
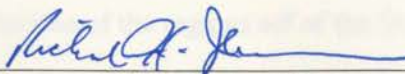Committee on Graduate Work

Wayne H. Schubert

David A. Krueger

Advisor: Thomas H. Vonder Haar

Co-Advisor: Steven D. Miller

Department Head: Richard H. Johnson

ABSTRACT OF THESIS

THREE REGIONAL CLIMATOLOGIES OF MARINE STRATOCUMULUS

CHARACTERISTICS USING THE A-TRAIN SATELLITE DATA

Low-level marine stratocumulus clouds are known to play a large role in the

Earth's radiation budget. They also present challenges to forecasts using numerical

models. While many studies have attempted to model or explain the complicated

microphysical aspects of these clouds, it is important to understand the broader

macrophysical relationships between the precipitation and radiative properties of marine

stratocumulus. In this thesis, data for these clouds over three subtropical regions has been

gathered for the time period spanning from June 15, 2006 to February 15, 2009. The data

come from NASA's A-train satellites, CloudSat, CALIPSO, and Aqua, and some of this

data is even compared to buoy observations off of the Pacific South American coast.

With marine boundary layer clouds defined by cloud top heights below 2 km in the

combined CloudSat-CALIPSO dataset, spatial and temporal averages are calculated for

cloud and precipitation frequency as the various combinations of cloud detection are

examined as well. Typical values for longwave and shortwave fluxes and cloud optical

depth are also obtained for one of the regions off of the South American coast, some of

which are compared to in-situ buoy data.

Lidar data from CALIPSO is key to detecting a majority of marine stratocumulus while the radar detects about 35% of marine stratocumulus. On average 12% of the marine stratocumulus are precipitating and this accounts for about 1/3 of the radar-detected clouds. Radar detection of marine stratocumulus and precipitation also increased for the nighttime passes. This research also shows the spatial and temporal seasonal and annual averages for cloud and precipitation amounts in each region. We found the South American region to be the cloudiest location with the most frequently precipitating marine stratocumulus. Marine stratocumulus clouds tend to increase the surface downwelling longwave flux by about 100 W m^{-2} with respect to clear sky while decreasing the downwelling shortwave flux by about 900 W m^{-2}. These estimated flux values only sometimes agree with nearby buoy data for the longwave fluxes and very rarely agree with the buoy shortwave fluxes, owing to spatial heterogeneity of the cloud field. Overall, the results provide new information about the precipitation processes of marine stratocumulus and its effects over an extended period of time for three subtropical locations.

Jessica A. Ram
Department of Atmospheric Science
Colorado State University
Fort Collins, CO 80523
Summer 2010

ACKNOWLEDGMENTS

State University under Cooperative Agreement W911NF-06-2-0015 with the Army

Research Laboratory.

Jessica A. Ram
Colorado State University
June 2010

TABLE OF CONTENTS

TABLE OF CONTENTS

1. INTRODUCTION

1.1 Background

Global cloud cover plays a fundamental role in the radiation budget of the Earth. It is important to sort out various contributions from each cloud type because of the varying cloud characteristics. Factors such as cloud depth, cloud composition, and liquid water content are just a few of the properties that greatly affect the radiation budget. In a changing climate, cloud climatologies are a necessity for understanding the overall effects of clouds, how clouds are changing with time, and provides insight into the possible role of clouds in the future climate. One category of cloudiness that receives particular attention is the marine stratocumulus decks in the subtropical regions. These clouds are widespread and persistent, and are present to varying degrees year round. They are of particular interest to the scientific community because of their negative impact on the radiation budget at the top of the atmosphere (TOA).

Marine stratocumulus are low level clouds that are composed entirely of liquid water. Both synoptic and mesoscale processes play a role in their formation and duration. While these clouds occur frequently over many global locations, the most commonly studied areas are the subtropical regions. Marine stratocumulus form here because of cooler sea surface temperatures (SSTs) and atmospheric subsidence. As part of the

1

Hadley cell circulation, solar heating causes the air to rise in the tropics and then subside in the subtropics where it produces a semi-permanent high pressure region along zonal bands between 15°-45° North and South. This large scale subsidence results in adiabatic warming that creates an inversion near the surface. This inversion contains the clouds within the lowest 2 km of the atmosphere. The areas of high pressure create winds that blow toward the equator in the subtropical regions. Ekman transport responds to the wind stress on the surface of the ocean and produces a current that moves 90° to the right (left) of the wind in the Northern (Southern) hemisphere. On both sides of the equator, this results in water being pushed away from the western shores of subtropical continental boundaries. Cooler water from below takes the place of the removed surface water and upwelling occurs. This process along with local ocean currents from higher latitudes contribute to cooler SSTs in three key subtropical regions: the Western coasts of North and South America and Africa. Cooler SSTs make for a stable boundary layer that is less susceptible to convective heating and more conducive to the formation of stratiform clouds.

Marine stratocumulus have a high albedo, meaning they reflect much of the incoming solar radiation. This is due to their high liquid water content. They also emit a similar amount of longwave radiation as the ocean surface because of their low height and warm temperatures. Hartmann et al., 1992, estimates that on average, low clouds reduce the TOA net radiation balance by 15 W m^{-2}. Changes in marine stratocumulus properties would then lead to a significant change in the overall regional and global radiation budgets. VanZanten and Stevens (2005) state that thinning of these clouds can lead to a decrease in the downwelling longwave radiation of 80 W m^{-2}. Randall et al.

2

(1984) estimates that a 4% increase in low cloud amount could offset global warming effects from a doubling of carbon dioxide, while Slingo (1990) estimates the necessary cloud amount to be more around 15 to 20%. It is important to understand the processes that govern the properties and processes of these clouds in order to better understand their current and future impact on the environment. While a great amount of work has been done looking into marine stratocumulus, there is still much to learn as current models are in need of improvement in order to properly represent these clouds. The current research adds to this growing knowledge base via the leveraging of new and unique satellite observations capable of sampling the vertical distribution of clouds and cloud properties.

1.2 Current Knowledge

With the combination of modeling, observational, and field campaign studies, our understanding of marine stratocumulus clouds has increased dramatically in the past few decades. Studies cover the range from aerosols (Petters et al. 2006; Twohy et al. 2005) to entrainment (Gerber et al. 2005; Zhang et al. 2004) to precipitation (vanZanten et al. 2005; Wood 2005a,b), but all aim to better our understanding of the formation and maintenance of marine stratocumulus.

Like many other cloud systems, marine stratocumulus are known to have both diurnal and seasonal cycles. Seasonal cycles vary by location, while all marine stratocumulus have a strongly pronounced diurnal cycle. Radiative cooling at night drives these clouds to expand and produce more precipitation than during the day.

3

A large factor that determines the radiative properties of these clouds involves the cloud's precipitation process. These clouds are known to drizzle very frequently even though most of the precipitation rarely reaches the surface because of evaporation in the subcloud layer. Rain rates produced by marine stratocumulus are typically measured in mm per day. Recent studies have proposed that drizzling could deplete the cloud of its liquid water content (Petters et al. 2006). A reduction in liquid water would reduce entrainment, alter the concentration of aerosols from the cloud layer, and ultimately change the clouds radiative properties (Stevens et al. 1998, Ackerman et al. 1993). However, the full extent of what makes these clouds drizzle and how the drizzle affects the clouds has yet to be fully understood, and hence is poorly resolved in models. VanZanten and Stevens (2005) state that during periods of intense drizzle at cloud base, the equivalent latent heat flux could be up to 145 W m^{-2}, creating a large impact on the energy budget below the cloud.

The formation of drizzle in marine stratocumulus has been found to promote a circulation favorable for open cell convection where broad regions of sinking motion are surrounded by narrow regions of rising motion. Figure 1.1 shows an example of open cell convection embedded within closed cell convection. This setup is characterized by pockets of thinner or open cloud surrounded by thicker cell walls that can be associated with heavy precipitation and have locally higher cloud tops. These pocket regions are commonly called pockets of open cells (POCs) from Stevens et al. (2005) after the second Dynamics and Chemistry of Marine Stratocumulus (DYCOMS-II) experiment, and tend to form in regions with larger droplet size and lower droplet concentration. Sharon et al. (2006) calls these cellular structures rifts, and states that they occur on the

4

scale of 10 to 20 km. An illustration representing the dynamic and thermodynamic properties of POC regions is shown in Figure 1.2. Precipitation from these areas is found to be greater than precipitation from closed cell marine stratocumulus. Without some moisture source, precipitation would only last on the timescale of minutes, yet these structures are known to precipitate on the timescale of a few hours. Regions that contain POCs also tend to have cooler and moister boundary layers, and therefore lower lifting condensation levels than non-POC regions (Stevens et al. 2005).

Figure 1.1 – A MODIS visible image from September 4, 2001 off of the Peruvian coast showing pockets of open cell convection inside closed cell marine stratocumulus (Located by Dr. Robert Wood at the University of Washington on the NASA Visible Earth website)

Figure 1.1 – *A MODIS visible image from September 4, 2003 off of the Peruvian coast showing pockets of open cell convection amidst closed cell marine stratocumulus [Located by Dr. Robert Wood at the University of Washington on the NASA Visible Earth website]*

POC Region ·· radiative export of θ_e

θ_e profile

z

10-20km

horizontal variation of θ_e

x
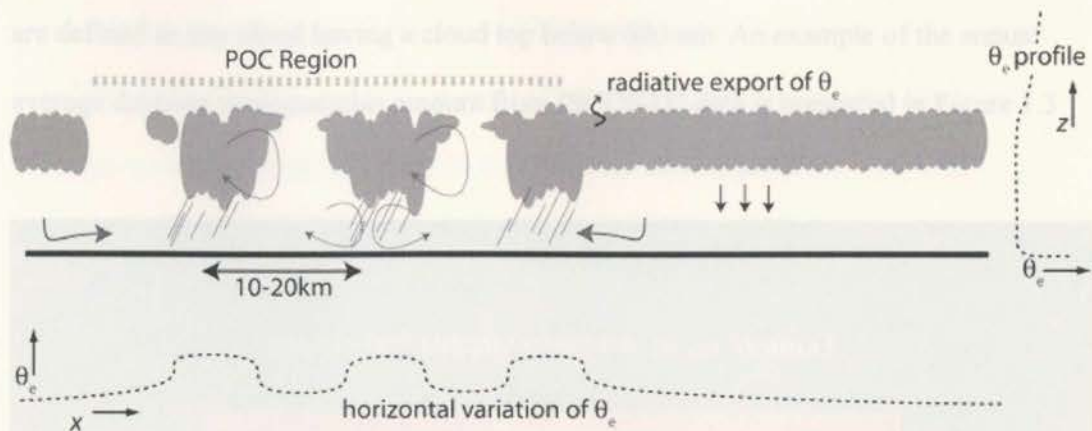
Figure 1.2 - A conceptual model of marine stratocumulus noting the variations in dynamics and thermodynamics for open and closed cell convection [Figure 10, vanZanten and Stevens 2005]

1.3 Climatologies

In order to understand the full impact on the Earth's energy budget we need to look at the climatologies of marine stratocumulus. Because of their occurrence over the ocean, very few surface based measurements exist and so these clouds are mostly observed using satellites. The examples provided below are by no means the only studies performed to observe long-term properties of low level clouds, but they are some of the more relevant to the purpose of this research.

One of the most popular satellite datasets for cloud climatologies is the International Satellite Cloud Climatology Project (ISCCP), which started in 1982. It uses global satellite measured radiance data to statistically calculate cloud fraction and cloud properties over a number of years applied to a 2.5° x 2.5° grid. In this dataset, low clouds

7

are defined as any cloud having a cloud top below 680 mb. An example of the annual

average daytime stratocumulus amount from ISCCP-D2 data is presented in Figure 1.3.

ISCCP-D2 198307-200806 Mean Annual
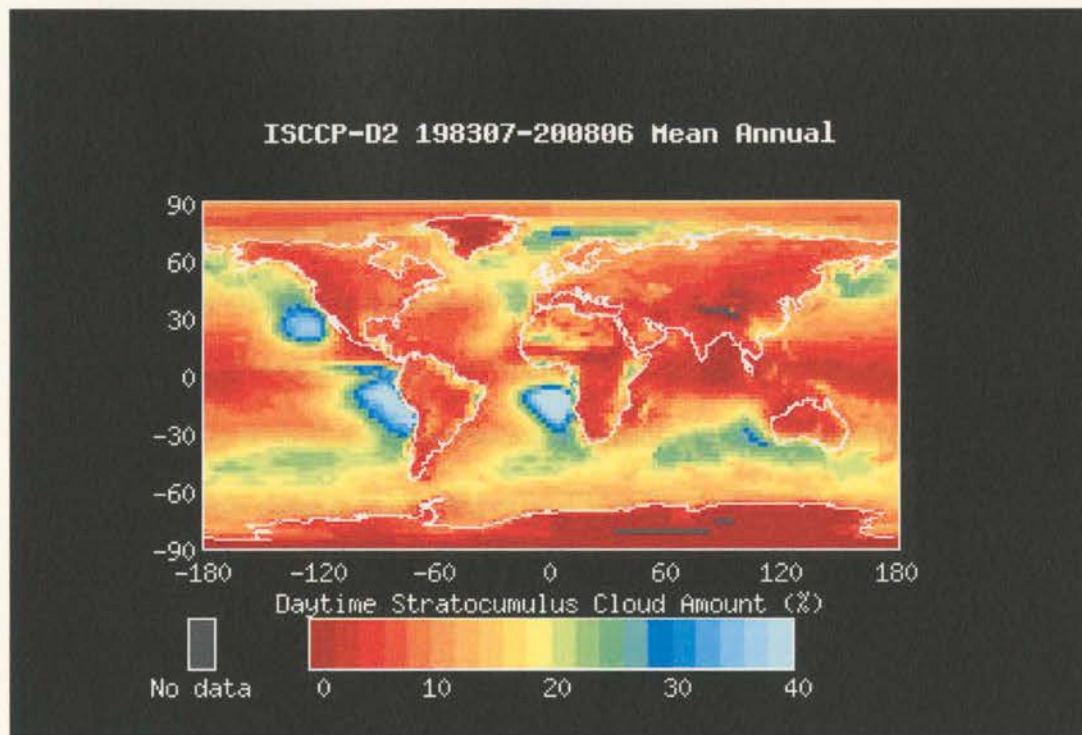
Figure 1.3 - The annual mean cloud amount for daytime stratocumulus [ISCCP website]

Much of the research pertaining to marine stratocumulus follows from a variety of

short-term field experiments and case studies, and so there is a need for increased long-

term observations. One of the more recent studies for this cloud type was in Leon et al.

(2008) where data from one year was used to create a global low cloud climatology on a

2.5° x 2.5° grid. They defined low clouds as any cloud with a cloud top below 4 km as

detected by the CloudSat or CALIPSO cloud masks. Rainrate was further calculated for

low clouds using a unique Z-R relationship. They found that the yearly averaged low

8

cloud fraction for the subtropical coasts of California, Namibia, and Peru were greater than 70% during the day and 85% at night. This study also concluded that the drizzle occurrence for these locations were 31%, 28%, and 34% respectively.

These three subtropical regions were also observed in Klein and Hartmann (1993) as regions where the cloud forcing was -40 W m^{-2} or less. The characterization of the influence of clouds on the earth's radiation budget in this study is obtained from the Earth Radiation Budget Experiment, described in detail by Barkstrom (1984). This paper also presents seasonal and annual averages for cloud amount gathered from routine weather observations and ship observations from cloud atlases given in Warren et al. (1986;1988), formatted to a 5° x 5° grid. Over the previously mentioned coastal regions, these results show annual stratus cloud amounts that exceed 50%.

1.4   Objective

Even with great strides in understanding the processes that help to shape marine stratocumulus, there is still a need to improve model parameterizations so that the characteristics of marine stratocumulus can be predicted and accurately represented in mesoscale, regional, and general circulation models (GCMs). The most recent Intergovernmental Panel on Climate Change Assessment Report (IPCC 2007) states that the representation of clouds in the present and future produces a large source of uncertainty in determining the sensitivity for current climate models. Some fairly accurate models are only performed over a small domain, and others fail to explain the details of the influence of precipitation.

9

Problems associated with GCMs in regions of marine stratocumulus include an underestimate of cloud amount leading to an overestimate of shortwave surface flux (Wyngaard and Moeng 1990), an increase in cloud amount resulting in unrealistic lowering of SSTs (Ma et al. 1996), or unrealistically thick clouds during the daytime (Zhang et al. 2005) to name a few. The more we can understand about the cloud characteristics from observations, the better chance there is of improving model forecast skill.

Much of the previous research involving marine stratocumulus has included modeling or field campaigns with relatively fewer long term observations. Increasing our observations of these clouds can only help to increase our understanding of what drives these clouds to form, precipitate, or dissipate. While the distribution of marine stratocumulus is fairly well known, few studies have been done to determine how frequently these clouds actually precipitate. Whether these clouds precipitate or not will undoubtedly affect the clouds radiative properties during different stages and formations of the clouds existence.

Because of the difficulty of gathering observations over the ocean, satellites play an enormous role in providing these observations. The goal of this research is to augment current observations of marine stratocumulus with several years of observations from an active satellite sensor dataset, and use surface observations from a buoy stationed under one of the stratocumulus decks to understand their radiative influences. Specifically, CALIPSO, CloudSat, and MODIS, are used to identify areas of cloud cover, precipitation, and radiative properties.

10

The three satellite sensors utilized in this research, CALIPSO's CALIOP,

CloudSat's CPR, and Aqua's MODIS, are described in Chapter 2. This is accompanied

by a description of the products derived from their data, along with a description of the

in-situ buoy data that is also used. Chapter 3 details the assumptions made in order to

apply the satellite and buoy data to this research. Results are then discussed in Chapter 4,

which consist of long term observations of various satellite detections of marine

stratocumulus cloud cover and precipitation, and radiative properties. Lastly, Chapter 5

interprets some of the more important conclusions that can be drawn from the results. An

important outcome of this research is a new dataset describing the precipitation

characteristics of subtropical marine stratocumulus clouds.

11

2. INSTRUMENTATION

2.1 Satellites/Sensors

The afternoon constellation of satellites (A-train) is a formation of five National Aeronautics and Space Administration (NASA) satellites that fly within 15 minutes of each other in order to provide near-simultaneous data. Satellites in the A-train include Aqua, CloudSat, CALIPSO, PARASOL, and Aura. It is called the afternoon constellation because of its sun-synchronous orbit where the satellites cross the equator at about 1:30 pm local time located at roughly 705 km in altitude. They orbit the globe about 14.5 times every day, and will repeat over the same path every 16 days. By combining the instrumentation and measurements from each satellite, this collaboration provides the scientific community with a wealth of information unlike any other dataset. The three A-train satellites used in this research are CloudSat, CALIPSO, and Aqua.

2.1.1 CloudSat/CPR

CloudSat joined the A-train on June 1, 2006. It is the first satellite with a millimeter wavelength cloud radar to fly in space. Its mission is to provide information of cloud structure, distribution, and radiative properties using the near-nadir-pointing cloud profiling radar (CPR) onboard the satellite.

12

The CPR sends a 3.3 μs pulse every 0.32 seconds giving CloudSat a vertical resolution of 250 m because of overlapping samples, and a horizontal resolution of 1.4 km cross track and along track. As a W-band radar with a frequency of 94 GHz, or a wavelength of 3 mm, the CPR has a relatively high sensitivity to cloud droplet-sized particles compared to other spaceborne radars which are more sensitive to precipitation-sized hydrometeors. The minimum detectable signal is about -30 dBZ, and this allows CloudSat to detect most of the cloud condensate and light precipitation such as drizzle in its field of view.

This research utilizes four data products that are available from the CloudSat Data Processing Center. These products include the combination of CALIPSO and CloudSat cloud masks in the Radar-Lidar Geometric Profile, estimation of rain rates from the Column Precipitation Algorithm, radiative flux measurements from the Fluxes and Heating Rates product, and collocated optical depth values from the Moderate Resolution Imaging Spectroradiometer (MODIS) sensor onboard Aqua.

2.1.2 CALIPSO/CALIOP

The Cloud-Aerosol Lidar and Infrared Pathfinder Satellite Observations (CALIPSO) satellite entered into the A-train constellation in May 2006 as part of NASA's Earth System Science Pathfinder program in collaboration with the Centre National d'Ètudes Spatiales, the French space agency. It was launched into orbit with CloudSat, and currently trails CloudSat by about 12.5 seconds in formation flight. CALIPSO's mission is to observe aerosol and cloud properties with the three sensors it

carries. The Cloud-Aerosol Lidar with Orthogonal Polarization (CALIOP) is CALIPSO's primary instrument, while two passive sensors, a wide field camera and an infrared imaging radiometer, provide additional swath data centered on the lidar footprint.

CALIOP is a two-wavelength polarization lidar that observes profiles in the troposphere and lower stratosphere. Because CALIOP can detect aerosols with a high resolution, this instrument works well in combination with the CPR on CloudSat due to its increased sensitivity and ability to detect optically thinner clouds. The lidar has a vertical resolution of 30 m and a horizontal resolution of 335 m. Profiles above 8.2 km are averaged because of the decreased likelihood of atmospheric spatial variability above this height. Due to its high sensitivity, the low signal-to-noise ratio requires more averaging in order to detect weakly scattering layers, which compromises the spatial resolution. It also means that attenuation from the upper atmosphere can reduce the sensitivity for profiles near the surface. Level 1 products from CALIOP contain profiles of attenuated backscatter, while level 2 products identify cloud and aerosol layers. Retrievals from the level 2 products are also fed into one of the CloudSat products discussed later on.

2.1.3 Aqua/MODIS

NASA's Aqua was launched on May 4, 2002 as the first satellite of the A-train, and currently flies one minute ahead of CloudSat. Its mission is to contribute to earth observations using six instruments: the Atmospheric Infrared Sounder (AIRS), the Advanced Microwave Sounding Unit (AMSU), the Humidity Sounder for Brazil (HSB),

14

the Advanced Microwave Scanning Radiometer for the Earth Observing System (AMSR-E), the Clouds and the Earth's Radiant Energy System (CERES), and MODIS. While each system has unique scientific contributions, only MODIS is used in this research to obtain cloud radiative and optical properties.

MODIS measures radiances from 36 different spectral bands with up to 250 m resolution, depending on the band. The MODIS swath is much larger than the CloudSat swath, spanning 2330 km. Radiances from this wide range of spectral bands are processed into a variety of products ranging from oceanic properties, to surface vegetation, to snow cover, to cloud and aerosol properties. Of interest to this research is the level 2 "MOD06" cloud product, described in detail in section 2.2.4.

2.2 Satellite Products

2.2.1 2B-GEOPROF-LIDAR

One of the most complete pictures of cloud and hydrometeor profile comes from combining the two main sensors on CloudSat and CALIPSO into the Level 2 Radar-Lidar Geometric Profile product (2B-GEOPROF-LIDAR). This combination of instruments takes advantage of the ability of the CPR to probe optically thick clouds that would normally attenuate the lidar signal, and the high sensitivity of the lidar to optically thin clouds and smaller hydrometeors that are beyond the sensitivity of the CPR. The spatial resolution for this combined product is driven by the resolution of the coarser CPR observations.

In order to obtain as much information as possible from the combination of these two sensors, the 2B-GEOPROF-LIDAR product calculates both a cloud fraction and cloud boundaries. The cloud fraction estimates the amount of a radar volume that is cloud filled. Because the radar beam spreads out as it propagates, about 9-10 separate lidar profiles contribute to one radar range bin below 8.2 km, and about 3-4 lidar profiles above 8.2 km (Mace 2007).

Cloud detection is provided by combining the cloud masks from both satellites. Up to five layers of cloud in each profile can be defined in this product, and each layer is defined by cloud top and cloud base heights. Each cloud top or base in a profile is marked by which sensor detected the hydrometeors, and this information is then stored as a contribution flag. Either the lidar, the radar, or both will detect a cloud boundary. Usually the lidar will detect the top most boundary in a layer because of its finer resolution and higher sensitivity. Following a cloud-free range level, the first level to contain over 50% cloudy lidar volumes is considered as the cloud boundary, and flagged as detected by the lidar. If the radar volume also detects hydrometeors, then the contribution flag would show that both the radar and the lidar detect the boundary. In certain cases there can be enough attenuation of the lidar beam so that only the radar will detect a boundary, and this is flagged as a radar-only detection. An example of the cloud layers defined in this product can be seen in Figure 2.1. This figure shows the different combinations of detection flags for both the cloud top and cloud base. It is also important to note that given this method, the product does not try to distinguish precipitation from cloud.
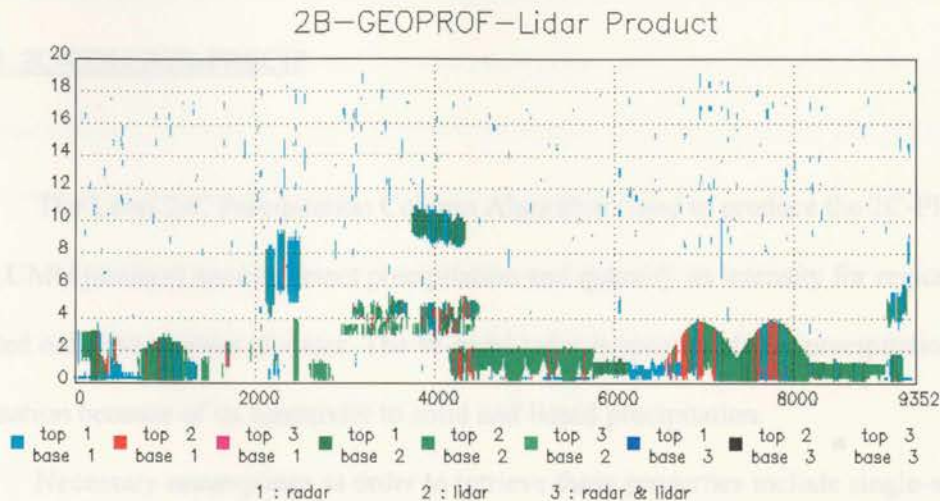
Figure 2.1 - An example of a profile from the 2B-GEOPROF-LIDAR where a flag of 1 is detected by the radar, 2 is detected by the lidar, and 3 is detected by both the radar and the lidar [Figure 4, Mace 2007]

The 2B-GEOPROF-LIDAR product is not without its caveats. One common issue

is misclassification by the lidar of dense aerosol layers as being cloud. The distinction

between cloud and aerosol for the lidar mask is about 90% accurate (Mace 2007). The

radar is sometimes not sensitive enough to detect some high thin ice clouds as well as

some non-precipitating water clouds. Issues with CPR-clutter also occur in the lowest 1

km due to reflection from the surface which reduces the ability to detect clouds. Clouds

below 500 m are likely to be missed, and only a subset of clouds below 1 km will be

found. One more mention is that during the nighttime, the lidar data becomes less noisy

and therefore detects more thin clouds than during the daytime. Despite these limitations,

the 2B-GEOPROF-LIDAR product still provides some of the best information on cloud

presence and vertical structure available from satellite remote sensing.

17

2.2.2 2C-COLUMN-PRECIP

The Level 2-C Precipitation Column Algorithm (used to produce the 2C-PRECIP-COLUMN product) aims to detect precipitation and quantify its intensity for regions located only over bodies of water. The W-band radar is appropriate for precipitation estimation because of its sensitivity to solid and liquid precipitation.

Necessary assumptions in order to retrieve these properties include single-scatter conditions, knowledge of the cloud droplet size distribution, and surface windspeed. The algorithm then uses Mie theory to estimate the path integrated attenuation (PIA), or the amount of power lost from the radar beam due to scattering and absorption. Using PIA as a constraint to estimate profiles of light to moderate rain was introduced in L'Ecuyer and Stephens (2002) where they concluded that a 94 GHz radar could produce accurate rainfall estimates.

The calculation of PIA is represented in equation 2.1 for a column with depth H.

$$PIA = 2\psi \int_0^H k_{ext}(s)ds \tag{2.1}$$

Scattering and absorption are represented as the extinction coefficient, k_{ext}, and this must be accounted for at every layer of the atmosphere. In the equation, ψ is a conversion factor equal to $10/\ln(10)$. In calculating the observed attenuation, the surface is by far the largest target that will scatter and absorb the radar beam, and so this can easily be detected and factored into the attenuation. Any reduction to the expected surface backscatter of a standard cloud free atmosphere is then due to attenuation from other gases, clouds, or precipitation. The algorithm must sort out the separate contributions

18

from each of these components. Gaseous attenuation is calculated with the help of the

vertical profile of temperature and moisture using data from the European Center for

Medium-Range Weather Forecasts (ECMWF) model. Attenuation due to clouds and

precipitation are determined using the assumption of a uniform vertical rain profile of

clouds defined by the 2B-GEOPROF cloud mask, and a Marshall Palmer drop size

distribution shown in equation 2.2 from Marshall and Palmer (1948). N is the particle

$$N(D) = N_0 \exp(-\lambda D)$$
$$\lambda = A_\lambda R^{B_\lambda}$$

(2.2)

number concentration and it has a dependence on the droplet diameter (D) and the

precipitation rate (R). N_0 is the intercept parameter of modified gamma distribution, 0.08

cm^{-4}, while A_λ and B_λ are parameters equal to 41 cm^{-1} and -0.21 respectively. Cloud

water content is also considered in a rainy profile using values from MODIS cloud

products.

The change in the expected PIA can only be calculated if the typical attenuation

values for clear sky conditions are known. In a standard cloud free atmosphere, the return

backscatter relies heavily on surface conditions. Over land, surface conditions depend on

vegetation, surface slope, soil moisture, snow cover, etc., while over the ocean surface

conditions depend mostly on surface wind speed, causing surface roughness, and SST.

For retrievals over ocean surfaces, surface winds are taken from AMSR-E onboard Aqua,

except when precipitation is present then ECMWF wind data are used. SST values are

also taken from ECMWF. Using this data, PIA can be accurately estimated to within 2

dB (Haynes et al. 2009). Surface conditions over land are much more difficult to

determine because of variability, and hence this algorithm does not attempt to quantify

these values.

19

The total observed attenuation is then matched to a predicted value of precipitation intensity. Any reflectivity below -15 dB is considered as a non-precipitating profile as shown in Table 2.1, and no retrieval is performed. A calculated PIA smaller than expected uses a Z-R relationship based on the assumed drop size distribution to calculate the precipitation rate. If the PIA is larger than expected, then the lookup table from Figure 2.2 is used to match that PIA with a precipitation rate. Overall, results from this retrieval using the W-band radar are most sensitive for smaller precipitation rates, meaning that this method works best for light rainfall (Haynes et al. 2009).

| Condition	Z_u Range (dB)
Rain definite	>0
Rain probably	-7.5 to 0
Rain possible	-15 to -7.5
Snow definite	>-5
Snow possible	-15 to -5
No precipitation	<-15

Table 2.1 - The liklihood of precipitation based on the unattenuated near-surface reflectivity, Z_u [Table 2, Haynes et al. 2009]

20
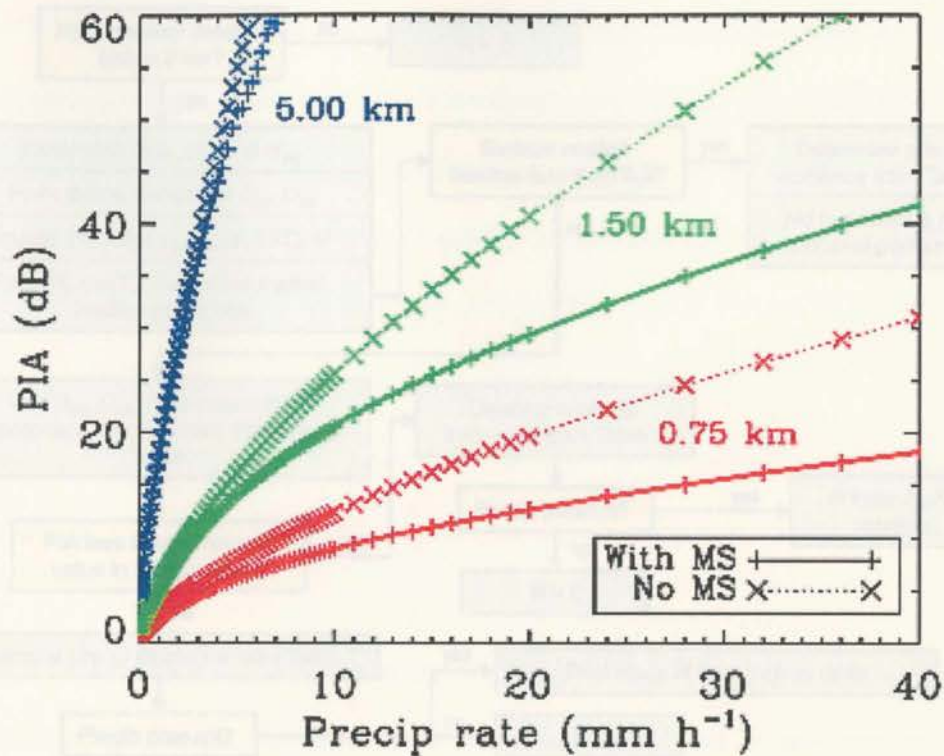
Figure 2.2 - Calculations of PIA as a function of rain rate with and without multiple scattering for various precipitating layer depths (shown in colors) [Figure 8, Haynes et al. 2009]

Other complications also exist for this algorithm, such as attenuation from different phases of precipitation and multiple scattering. The presence of a melting layer means that hydrometeor extinction will vary with height. Also, during snow or heavy precipitation events, photons from the radar beam may scatter off of more than one target before reaching the receiving antenna. Both of these issues are accounted for in this product, and can be found in further detail in Haynes et al. (2009), but for the case of light warm rain in marine stratocumulus, these processes are negligible. A complete summary of the rainfall retrieval algorithm is shown in Figure 2.3.
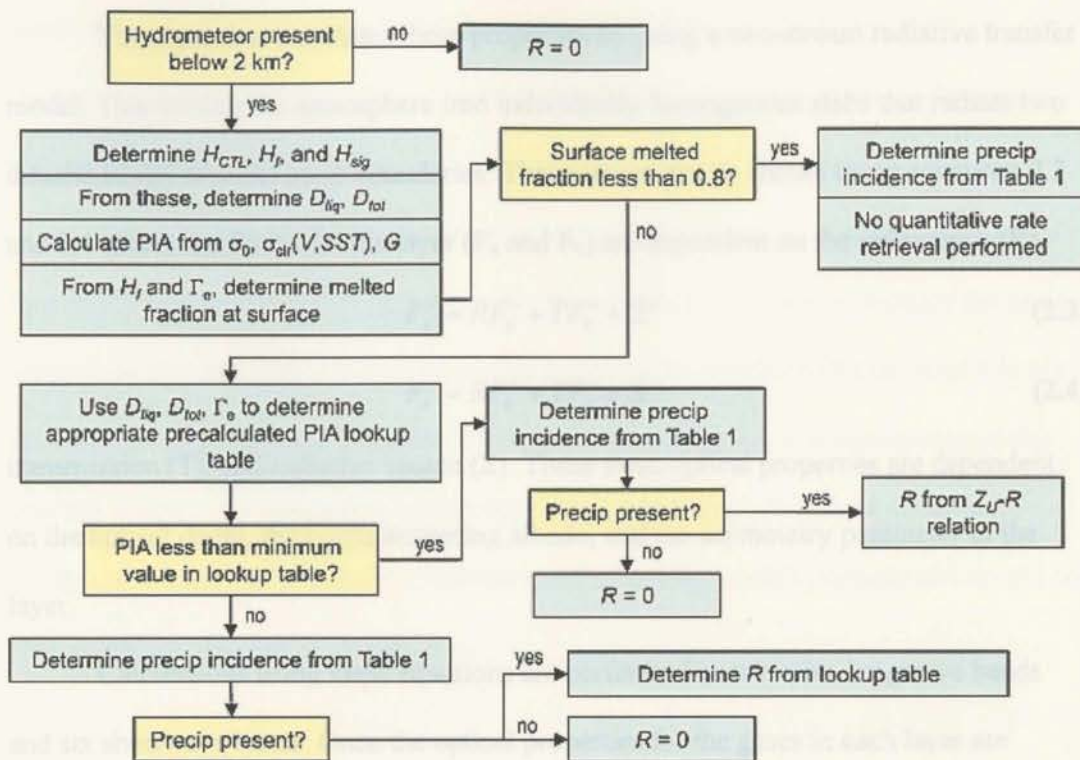
Figure 2.3 - *Then flowchart for the full rainfall retrieval algorithm [Figure 7, Haynes et al. 2009]*

2.2.3 2B-FLUX

The Level 2 Fluxes and Heating Rates product, 2B-FLXHR, uses the liquid and ice water contents from the CPR to infer radiative properties of the atmosphere. This product provides estimates of broadband fluxes and heating rates for each radar bin by calculating upwelling and downwelling fluxes that can then be used to calculate heating rates for both longwave and shortwave radiation.

22

The algorithm calculates these properties by using a two-stream radiative transfer model. This divides the atmosphere into individually homogenous slabs that radiate two dimensionally from its layer boundaries. This concept can be shown using equations 2.3 and 2.4 where the fluxes for the layer (F_a and F_b) are dependent on the reflectance (R),

$$F_a^+ = RF_a^- + TF_b^+ + \Sigma^+ \tag{2.3}$$

$$F_b^- = RF_b^+ + TF_a^- + \Sigma^- \tag{2.4}$$

transmission (T), and radiative source (Σ). These three optical properties are dependent on the optical depth, the single scattering albedo, and the asymmetry parameter of the layer.

Calculations using these equations are performed over twelve longwave bands and six shortwave bands. Once the optical properties for the gases in each layer are determined, the cloud optical properties are combined with the atmospheric optical properties, which are then fed into the two-stream calculations explained above. The resulting spectral fluxes are added to determine broadband fluxes, from which heating rates are computed. The final product is formatted for the CPR's resolution with vertical bins of about 240 m.

The initial retrieval of optical properties entails gathering data for ice water and liquid water contents from the CloudSat 2B-CWC product, atmospheric state variables from the ECMWF-AUX product, reflection properties from the CloudSat ancillary albedo product, and solar zenith angle from the MODIS-AUX product. If the 2B-CWC product is unavailable then the fluxes cannot be calculated. In the cases where cloud water content cannot be retrieved in precipitation, a large liquid water content is assumed. This causes slightly greater uncertainty in the fluxes for raining scenes. When liquid

23

water and ice water can be retrieved, their distributions are assumed to be uniform throughout a cloudy layer. Further assumptions and data descriptions can be found in L'Ecuyer (2007).

Because of its dependence on a number of different inputs, a status flag is provided for every profile to further explain the calculation. However, because the main inputs into the algorithm are from CloudSat products, the computed fluxes stored in this product are only applicable to radar-detected clouds. Currently, a newer version of this product is being developed that will include cloud and aerosol data from CALIPSO, along with MODIS cloud optical properties and CloudSat rainfall products to improve the representation of cloud properties.

2.2.4 MOD06-1KM-AUX

The MOD06 Cloud Product is a Level 2 product processed from MODIS radiances. The MOD06-1KM-AUX product is created by the CloudSat Data Processing Center and uses only the pixels that are closest in location to the CloudSat footprint from the original MOD06 data. The MOD06 products are produced, and include 1 km resolution information on cloud top temperature, height, and emissivity, cloud particle phase, cloud fraction, and three cloud optical properties: cloud water path, optical thickness, and effective radius (r_e). The cloud optical depth is the focus for this research because of its direct influence on the radiation reaching the surface.

The overlying concept for calculating optical depth and particle size simultaneously is that the reflection from clouds at a nonabsorbing visible band is

24

primarily a function of optical depth while reflection at an absorbing near-infrared band is primarily a function of particle size. Calculations of optical depth over oceans use one visible band, 0.858 μm, and three near-infrared bands, 1.64, 2.13, and 3.75 μm (King et al. 1997). Once the MODIS data has been screened by the cloud mask of Ackerman et al. (1997) and particle phase information is gathered from the algorithm of Menzel and Strabala (1997), the reflected intensity field is calculated using a radiative transfer model. The reflective properties of a layer depend mostly on the scaled optical thickness, r_e, and the albedo of the underlying surface. Then this value must be weighted by the band's spectral response and the incoming solar flux. The measured reflectances are then compared to simulated reflectance's provided as a function of optical depth and r_e in a lookup table. Testing of this table further shows that under optically thick conditions, optical depth and r_e are nearly independent of eachother (King et al. 1997). Currently, these two properties are being retrieved separately using bands with the appropriate sensitivity.

Uncertainties in this algorithm can come from uncertainties in the model used or in the physical quantities. The model can introduce slight errors if it does not adequately account for the variability of optical constants with wavelength, such as varying values of the real and imaginary parts of the complex refractive index. This problem can occur because considering less wavelengths will reduce the complexity of the computations. Errors in the physical quantities can arise from either changing quantities or from instrument calibration.

One of the largest limitations to using this product is that because of the need to measure the reflected intensity field at visible and near-infrared wavelengths, values for

25

optical depth can only be retrieved during daytime swaths. Another limitation occurs because the retrieval provides a calculation for a single-layer liquid water cloud that is horizontally and vertically homogeneous, causing further uncertainties when ice clouds or clouds with horizontal and vertical variations are present. And lastly, the sensitivity for these retrievals is reduced in the presence of shadows and large solar zenith angles.

2.3 In-situ Buoy Data

In order to improve our understanding of the surface fluxes under marine stratocumulus, The Woods Hole Oceanography Institute's Upper Ocean Process group deployed a buoy in October 2000 at 20°S, 85°W under the South American stratus deck. An image of the current buoy in place is displayed in Figure 2.4. As an Ocean Reference Station, this buoy provides many years of data that is useful to climate observations and models. This station is key to understanding the forcings and ocean-atmosphere interactions in this location by providing in-situ measurements for sparsely sampled oceanic region. About once a year, this site is maintained by replacing the three 3 m discus buoy and instrumentation.

26

Figure 2.4 - *An image of the current Woods Hole Oceanographic Institute's Ocean Reference Station taken in January 2010*

Instruments onboard the buoy include a stream of oceanographic instruments throughout the mooring line, along with two sets of the Air-Sea Interaction Meteorology (ASIMET) system. Measurements from the ASIMET system are from meteorological and sea surface sensors that calculate properties such as air temperature, SST, barometric pressure, relative humidity, wind speed and direction, precipitation, and incoming short and longwave radiation recorded every minute. Only the broadband radiative fluxes were used in this research.

The radiation sensors are raised on a platform so that they are not shaded by the other instruments. Shading can occur at low sun angles when the shade is produced by the instrument itself although this does not coincide with the timing of the A-train overpasses. Longwave radiation is measured using an Eppley precision infrared radiometer (PIR) that consists of a thermopile and one dome thermistor and one case thermistor. The measured thermopile voltage and the dome and case temperatures are used to compute the incoming longwave radiation. Shortwave radiation is measured with an Eppley precision spectral pyranometer (PSP), which has a wire-wound thermopile and a double glass dome. The voltage output from the thermopile is calibrated to compute shortwave radiation.

Concerns with the longwave sensor on a buoy at sea include contamination from solar radiation, tilt effects, thermal gradients within the dome and case temperatures due to differential heating, and dome contamination, which can include salt spray crystallization or bird guano (Colbo and Weller 2009). Shortwave measurements can also be compromised by tilting effects or thermal gradients within the dome. In order to ensure the sensors' accuracy, lab calibrations are examined far beforehand and then testing phases ensue in the weeks prior to deployment. Estimates of the possible error contributions for the longwave and shortwave sensors from various effects are shown in Tables 2.2 and 2.3 as calculated by Colbo and Weller (2009).

Precision	Lab calibration	Drift	Field errors	Total
Dome temperature: 0.1°C Case temperature: 0.1°C Thermopile: 10 μV	Coef: 1.5 W m^{-2} Noise: 0.5 W m^{-2}	2 W m^{-2}	Tilt: <2 W m^{-2} Temperature gradients: 4 W m^{-2} Salt spray: <1 W m^{-2} Solar: <1% SW↓	Instant: 7.5 W m^{-2} Daily: 4 W m^{-2} Annual: 4 W m^{-2}

Table 2.2 - *Estimated instantaneous errors for the longwave sensor for one-minute measurements, daily averages, and annual averages [Table 2, Colbo and Weller 2009]*

| Precision	Lab calibration	Drift	Field errors	Total
0.1 W m^{-2}	2 W m^{-2}	<2 W m^{-2}	Tilt: <2% Temperature gradients: 1-2 W m^{-2} Salt spray: <1 W m^{-2}	Instant: 20 W m^{-2} (more in broken cloud) Daily: 6 W m^{-2} Annual: 5 W m^{-2}

Table 2.3 - *Estimated instantaneous errors for the shortwave sensor for one-minute measurements, daily averages, and annual averages [Table 3, Colbo and Weller 2009]*

3. METHODOLOGY

3.1 Spatial and Time Domain

In order to observe multiple seasons of marine stratocumulus, data for this research spans from June 15, 2006, the beginning of the CloudSat mission, to February 15, 2009, providing about 32 consecutive months of data. These dates were chosen in order to maximize the amount of data available while the research was conducted. While the occasional missing profile can be expected, larger processing errors with the CloudSat data occurred from December 6-19, 2006, November 5-8, 2007, March 3-10, 2008, and June 4-10, 2008. A plot showing the number of profiles in the dataset for each month is presented in Figure 3.1.

Total Monthly Profiles
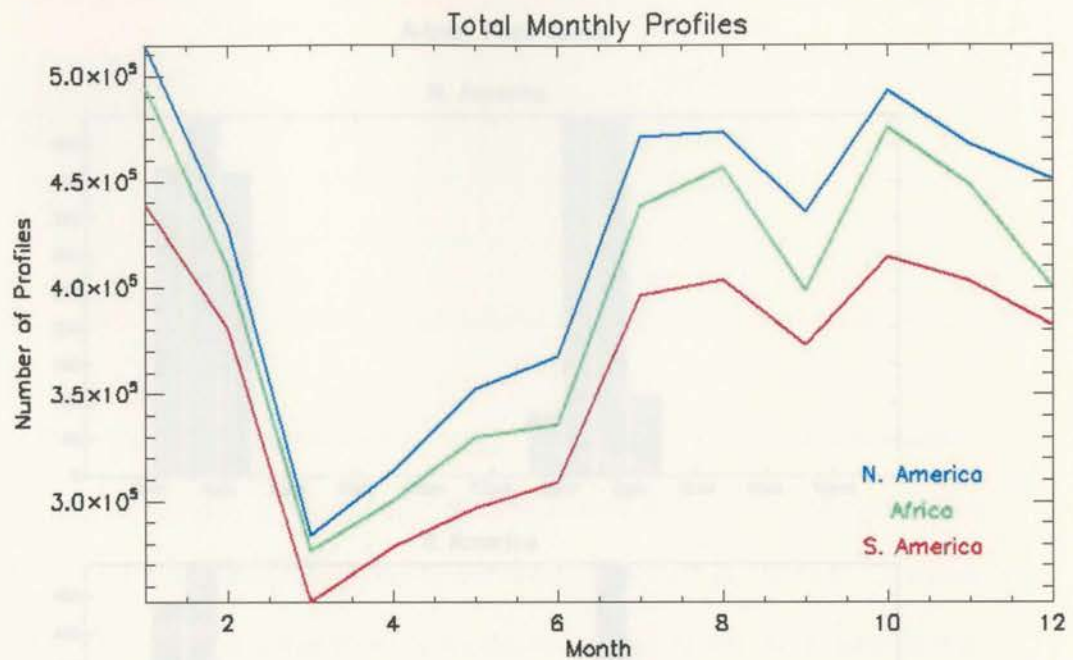
Figure 3.1 - *The total number of profiles in the dataset for each month in all three locations*

Because the A-train follows a sun-synchronous orbit, all passes are made around the same two local times for any given location. Figure 3.2 shows the local time for all of the passes at the three locations studied in this research. The time of the first profile within the bounded region is considered for each pass. The time zones considered for each region is indicated in Table 3.1. All passes are within about two or three hours of any other given pass for either the day or night. This is important to keep in mind when considering the day-night statistics for precipitation since the A-train does not sample the diurnal cycle uniformly.

31
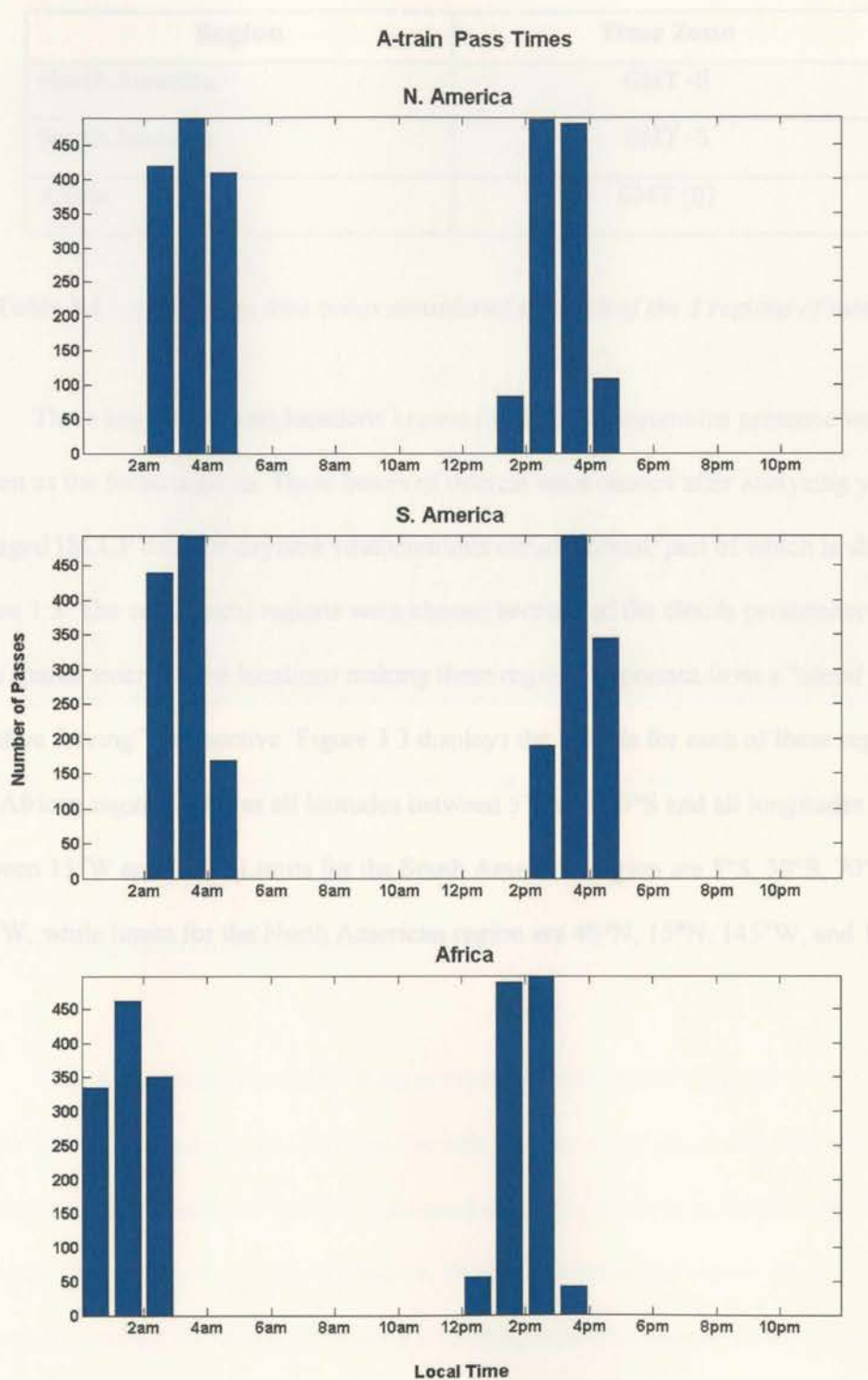
Figure 3.2 - Histogram of the local time of satellite passes for each location

Region	Time Zone
North America	GMT -8
South America	GMT -5
Africa	GMT (0)

Table 3.1 - *A list of the time zones considered for each of the 3 regions of interest*

Three key subtropical locations known for their stratocumulus presence were chosen as the focus regions. These boxes of interest were chosen after analyzing yearly averaged ISCCP data for daytime stratocumulus cloud amount, part of which is shown in Figure 1.3. The subtropical regions were chosen because of the clouds persistence and large spatial extent in the locations making these regions important from a "cloud radiative forcing" perspective. Figure 3.3 displays the bounds for each of these regions. The African region includes all latitudes between 5°S and 30°S and all longitudes between 15°W and 15°E. Limits for the South American region are 5°S, 30°S, 70°W, and 100°W, while limits for the North American region are 40°N, 15°N, 145°W, and 110°W.
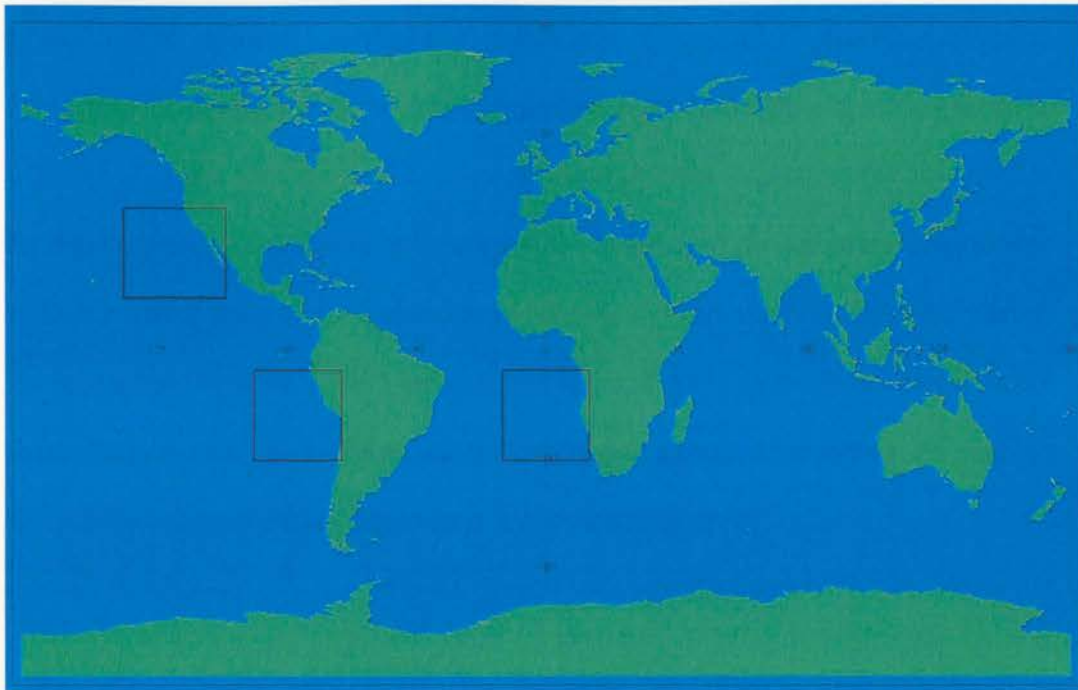
Figure 3.3 - Boxes showing the three subtropical regions of study used in this research

3.2   Defining Marine Stratocumulus

One of the greatest benefits of combining CloudSat and CALIPSO data is that the

marine stratocumulus can almost always be detected by one of the sensors. However,

limiting the classification of these clouds using only the variables in the dataset creates a

challenge. The aim is to include the bulk of these low level water clouds while at the

same time weeding out unwanted signals from other mid-level disturbances or convective

systems. Marine stratocumulus in this thesis is defined as any clouds defined by the 2B-

GEOPROF-LIDAR product having a cloud top height below 2 km, and the cloud must

occur over the ocean. One of the variables within almost every CloudSat product is labeled "DEM_elevation", or digital elevation map. This variable records the elevation of the surface, assigning a value of -9999 for profiles over the ocean, and so only profiles with this value are considered. A maximum height of 2 km is a commonly accepted level for these clouds, and as shown in Figure 3.4, the majority of marine stratocumulus are included. Any marine stratocumulus cloud beneath another cloud that filled any part of the atmosphere between 3 and 5 km was also factored out to ensure that a signal return below 2 km is not a result of elevated precipitation or a convective system. An example of a profile before and after this process is shown in Figure 3.5.
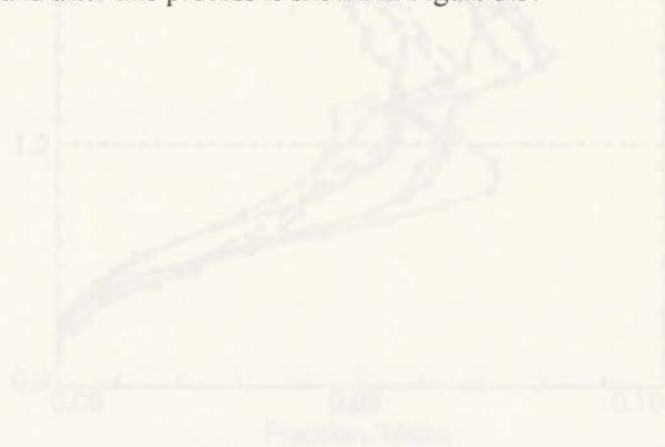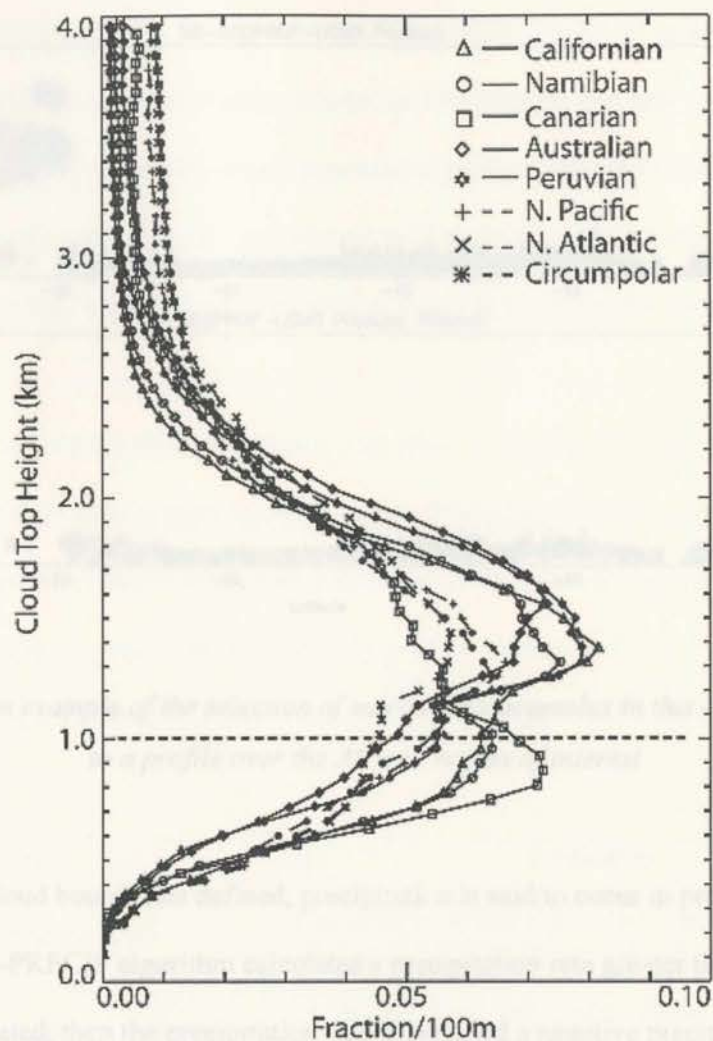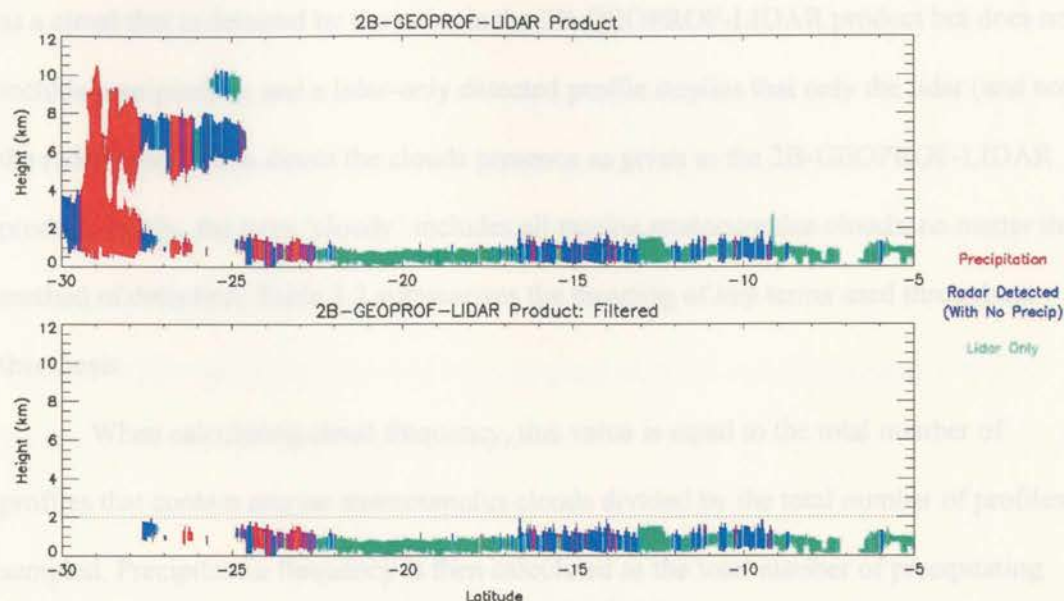

Figure 3.4 - Cloud top heights derived from CALIPSO for various stratocumulus regions. (Figure 6 Leon et al. 2008)

Figure 3.4 - *Cloud top heights derived from CALIPSO for various stratocumulus regions [Figure 1, Leon et al. 2008]*

2B-GEOPROF-LIDAR Product

2B-GEOPROF-LIDAR Product: Filtered

Precipitation

Radar Detected
(With No Precip)

Lidar Only

Figure 3.5 - *An example of the selection of marine stratocumulus in this research applied to a profile over the African region of interest*

With cloud boundaries defined, precipitation is said to occur in profiles where the 2C-COLUMN-PRECIP algorithm calculates a precipitation rate greater than zero. If the profile is saturated, then the precipitation rate is assigned a negative precipitation rate, for which the absolute value of this is the maximum retrievable precipitation rate by CloudSat, and this profile is counted as precipitating. Initially it was thought that the radar detection of a low level cloud as shown in the 2B-GEOPROF-LIDAR data was sufficient to flag precipitation. This hypothesis however was eventually rejected after comparison between the 2C-COLUMN-PRECIP and 2B-GEOPROF-LIDAR products, which will be further described in Chapter 4. The initial hypothesis however led to a useful analysis of sensor-specific cloud/rain detection. For the rest of this thesis, a precipitating profile is defined from the PIA algorithm, a radar-detected profile is defined

as a cloud that is detected by the radar in the 2B-GEOPROF-LIDAR product but does not include precipitation, and a lidar-only detected profile implies that only the lidar (and not the radar) was able to detect the clouds presence as given in the 2B-GEOPROF-LIDAR product. Lastly, the term 'cloudy' includes all marine stratocumulus clouds, no matter the method of detection. Table 3.2 summarizes the meaning of key terms used throughout this thesis.

When calculating cloud frequency, this value is equal to the total number of profiles that contain marine stratocumulus clouds divided by the total number of profiles sampled. Precipitation frequency is then calculated as the total number of precipitating profiles divided by the total number of cloudy profiles. Averages for both are provided for each location annually, seasonally, and for night and day.

Term	Definition
Marine stratocumulus	Cloud layer within the lowest 2 km with no cloud between 3-5 km above, located over the ocean
Precipitation	Precipitation rate greater than 0 in a marine stratocumulus profile
Radar-detected profile	Radar detection anywhere in the marine stratocumulus cloud that is not precipitating
Lidar-only detected profile	A marine stratocumulus profile that is only detected by the lidar
Cloudy	A profile containing a marine stratocumulus cloud
Cloud Frequency	The number of profiles containing marine stratocumulus / the total number of profiles
Precipitation Frequency	The number of precipitating profiles / the number of profiles containing marine stratocumulus

Table 3.2 – *A summary of all "definitions" as used in the present study*

38

A 1.5° x 1.5° grid is used to collect and show some of these results. It is not possible for a sun-synchronous non-scanning sensor to sample the entire surface of the earth uniformly. Figure 3.6 shows an example of the CPR tracks over the North American region with a 0.1° x 0.1° resolution. In order for the sampling to be uniformly distributed over all three regions with the finest possible resolution, a 1.5° x 1.5° grid is necessary. This will ensure that the future displays of cloud and precipitation frequency are tied to physics and not from sampling artifacts.

A-train Passes
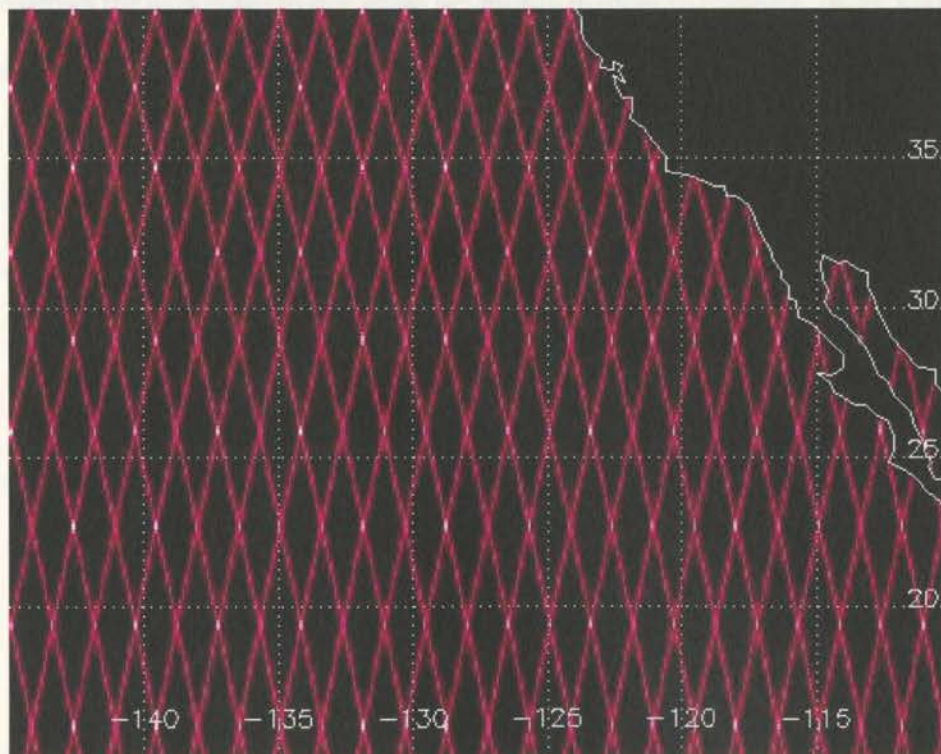
Figure 3.6 - *A map showing the location of the repeating track of A-train passes off of the North American coast with 0.1° x 0.1° resolution*

3.3 Determining Fluxes

Only radiative flux data for the South American focus region are considered in this thesis. This allows for an analysis of cloud radiative properties where additional data from the buoy is available as a source of validation. The 2B-FLXHR product provides a vertical distribution of shortwave and longwave radiative fluxes and radiative heating/cooling rates. However, in this thesis only the downwelling fluxes at the surface are considered. The interest for this research is in the marine stratocumulus effects on the surface values of these fluxes, and so fluxes are taken from the first bin above the surface. This narrows the data down to one value per profile in order to compare 2B-FLXHR flux values to both cloud optical depth and surface observations from the buoy.
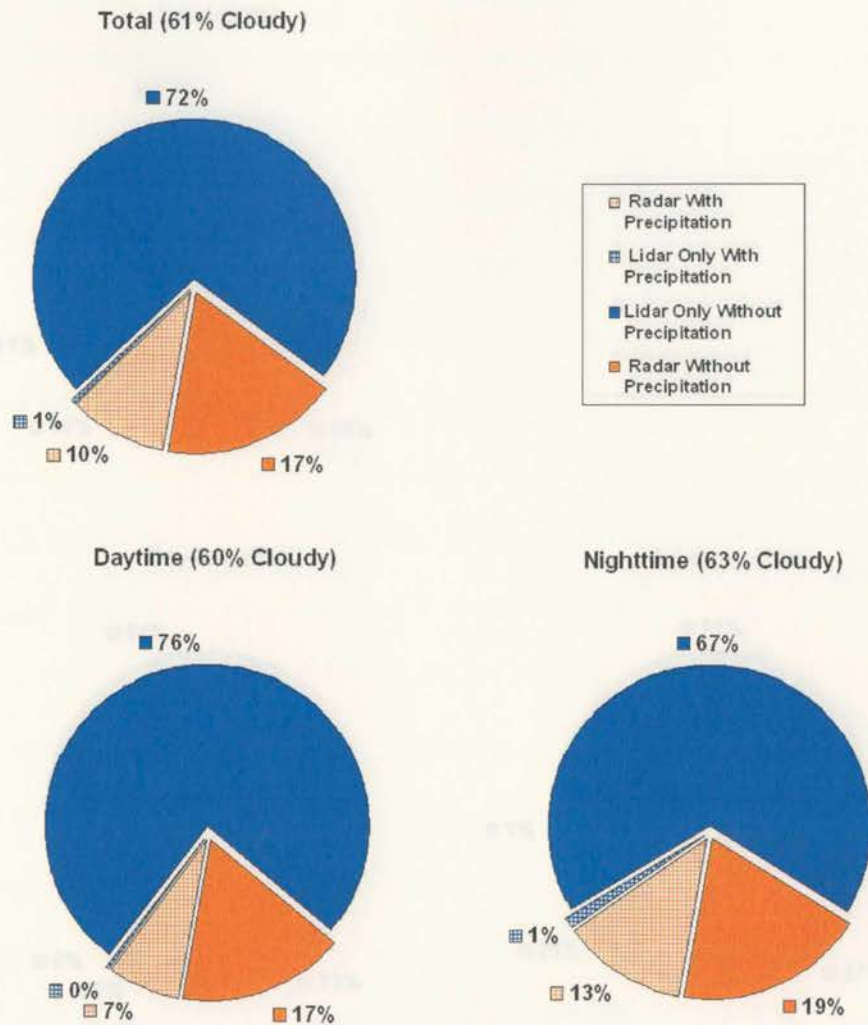
40

4. RESULTS

4.1 Cloud and Precipitation Statistics

Before any other analysis of these clouds, it is necessary to know how all of these sensors and products view marine stratocumulus. Figures 4.1, 4.2, and 4.3 show that in each subtropical region, marine stratocumulus in the 2B-GEOPROF-LIDAR product are detected by either (a) the radar, which could also be detected by the lidar, or (b) only the lidar, where most cloud droplets are too small or sparse to provide a radar signal. A portion of both scenarios can also be precipitating. In every region the lidar is the only sensor to observe the majority of the clouds, and less than 1% of these profiles contain precipitation according to the PIA algorithm. The radar is able to detect around 30-35% of the marine stratocumulus, with the PIA algorithm calculating precipitation in about 36% of these radar-detected profiles. This means that about 2/3 of the marine stratocumulus clouds detected by the CPR do not contain precipitation. Overall, the average precipitation frequency of marine stratocumulus is about 12%. As the figures show, a very small portion of precipitating marine stratocumulus are missed by the radar, appearing in the "Lidar Only With Precipitation" category. During the nighttime passes, radar detection increases and precipitation nearly doubles from the daytime passes.
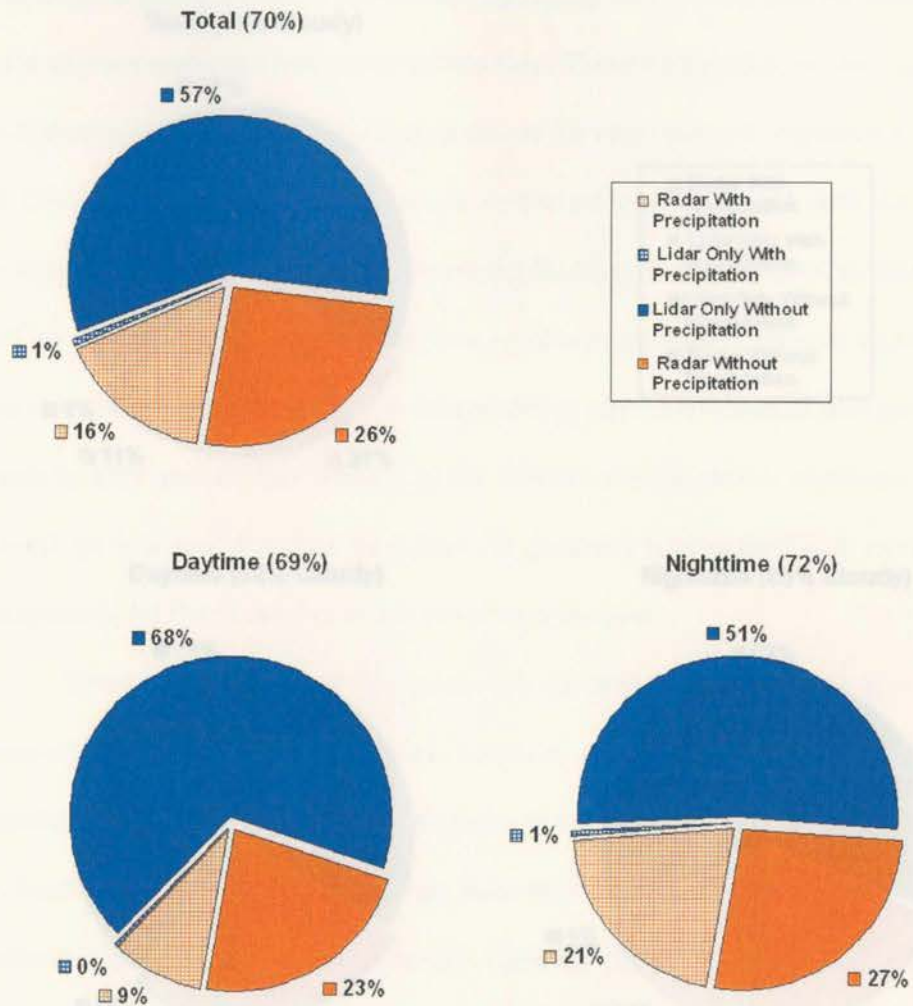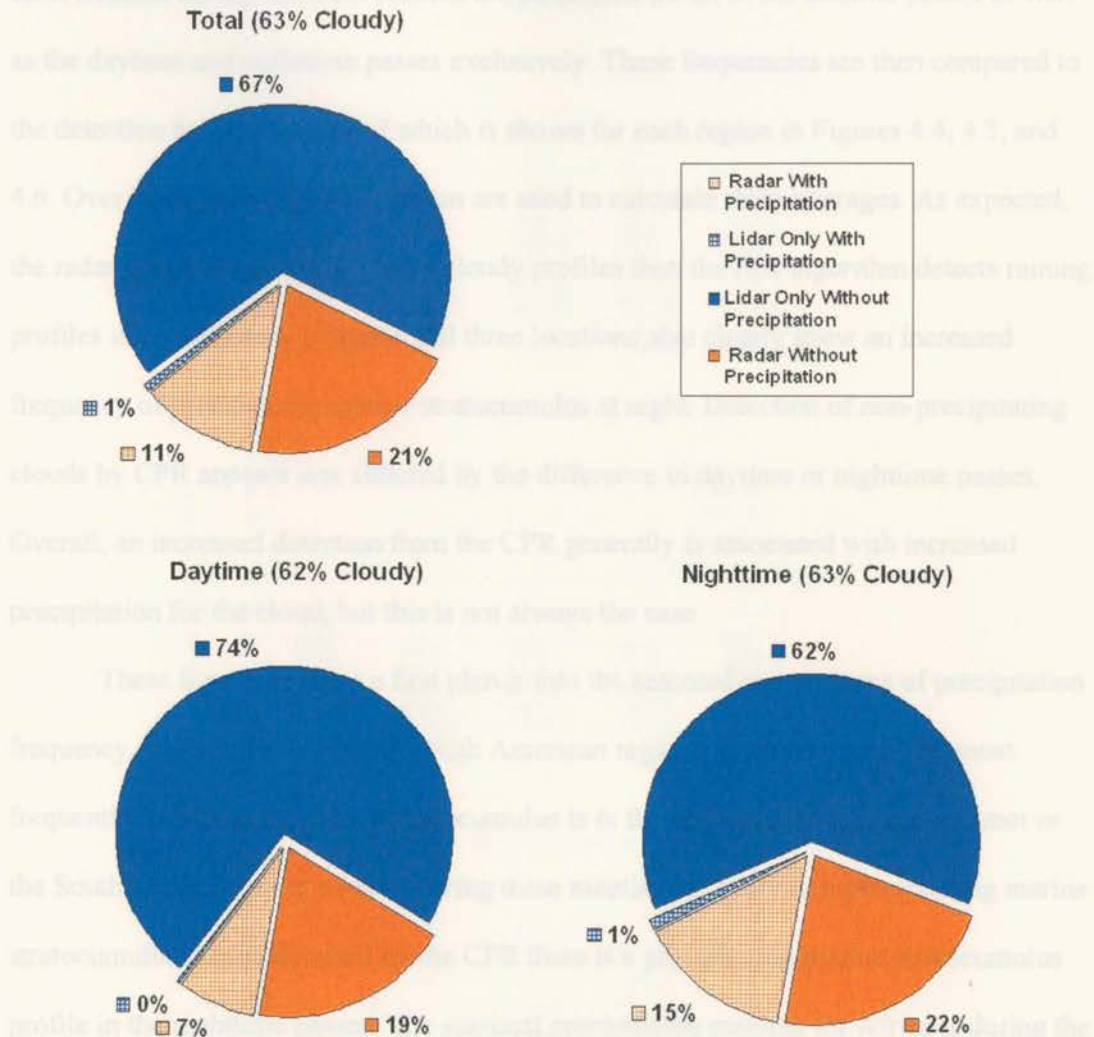
Total (61% Cloudy)

■72%

□ Radar With
   Precipitation
⊞ Lidar Only With
   Precipitation
■ Lidar Only Without
   Precipitation
■ Radar Without
   Precipitation

⊞1%
□10%   ■17%

Daytime (60% Cloudy)   Nighttime (63% Cloudy)

■76%   ■67%

⊞ 0%   ⊞1%
□ 7%   ■17%   □13%   ■19%

Figure 4.1 - *Sensor detection and precipitation of marine stratocumulus for the*
percentage of cloudy profiles in the North American region during the daytime,
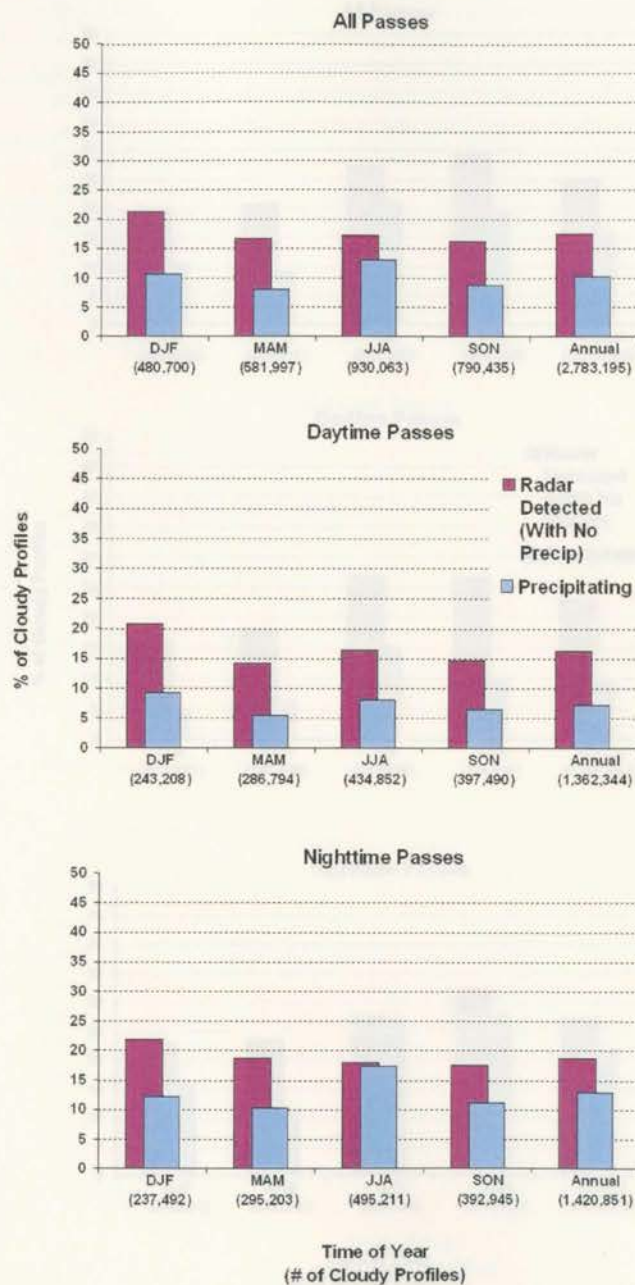*nighttime, and all passes*

S. America: Detection of Cloudy Profiles

Total (70%)

- 57%
- 1%
- 16%
- 26%

Legend:
- ☐ Radar With Precipitation
- ⊞ Lidar Only With Precipitation
- ■ Lidar Only Without Precipitation
- ■ Radar Without Precipitation

Daytime (69%)

- 68%
- 0%
- 9%
- 23%

Nighttime (72%)

- 51%
- 1%
- 21%
- 27%

Figure 4.2 - *Sensor detection and precipitation of marine stratocumulus for the percentage of cloudy profiles in the South American region during the daytime, nighttime, and all passes*

43

Africa: Detection of Cloudy Profiles

Total (63% Cloudy)

67%

1%

11%

21%

Radar With Precipitation

Lidar Only With Precipitation

Lidar Only Without Precipitation

Radar Without Precipitation

Daytime (62% Cloudy)

74%

0%

7%

19%

Nighttime (63% Cloudy)

62%

1%

15%

22%

Figure 4.3 - *Sensor detection and precipitation of marine stratocumulus for the percentage of cloudy profiles in the African region during the daytime, nighttime, and all three locations have the least amount of*

passes

With this information, the precipitation frequency of marine stratocumulus for each location during different seasons are calculated for all of the satellite passes as well as the daytime and nighttime passes exclusively. These frequencies are then compared to the detection by the CPR, all of which is shown for each region in Figures 4.4, 4.5, and 4.6. Over 2000 passes for each region are used to calculate these averages. As expected, the radar detects significantly more cloudy profiles than the PIA algorithm detects raining profiles in almost every scenario. All three locations also clearly show an increased frequency of precipitating marine stratocumulus at night. Detection of non-precipitating clouds by CPR appears less affected by the difference in daytime or nighttime passes. Overall, an increased detection from the CPR generally is associated with increased precipitation for the cloud, but this is not always the case.

These figures are also a first glance into the seasonal comparisons of precipitation frequency. In both the North and South American regions, the season with the most frequently precipitating marine stratocumulus is in the Northern hemisphere summer or the Southern hemisphere winter. During these months, for every non-precipitating marine stratocumulus profile detected by the CPR there is a precipitating marine stratocumulus profile in the nighttime passes. The seasonal precipitation maxima for Africa is during the Southern hemisphere spring. Out of the three locations, South America clearly has the most frequently precipitating marine stratocumulus. During March, April, and May, all three locations have the least amount of precipitation despite the fact that the northern and southern hemispheres are opposite in season.

45

N. America: Detection Frequency

All Passes

Daytime Passes

% of Cloudy Profiles

Nighttime Passes

Time of Year
(# of Cloudy Profiles)

*Figure 4.4 - The percentage of profiles over the North American region that are
precipitating or radar-detected without precipitation for seasonal and annual averages,
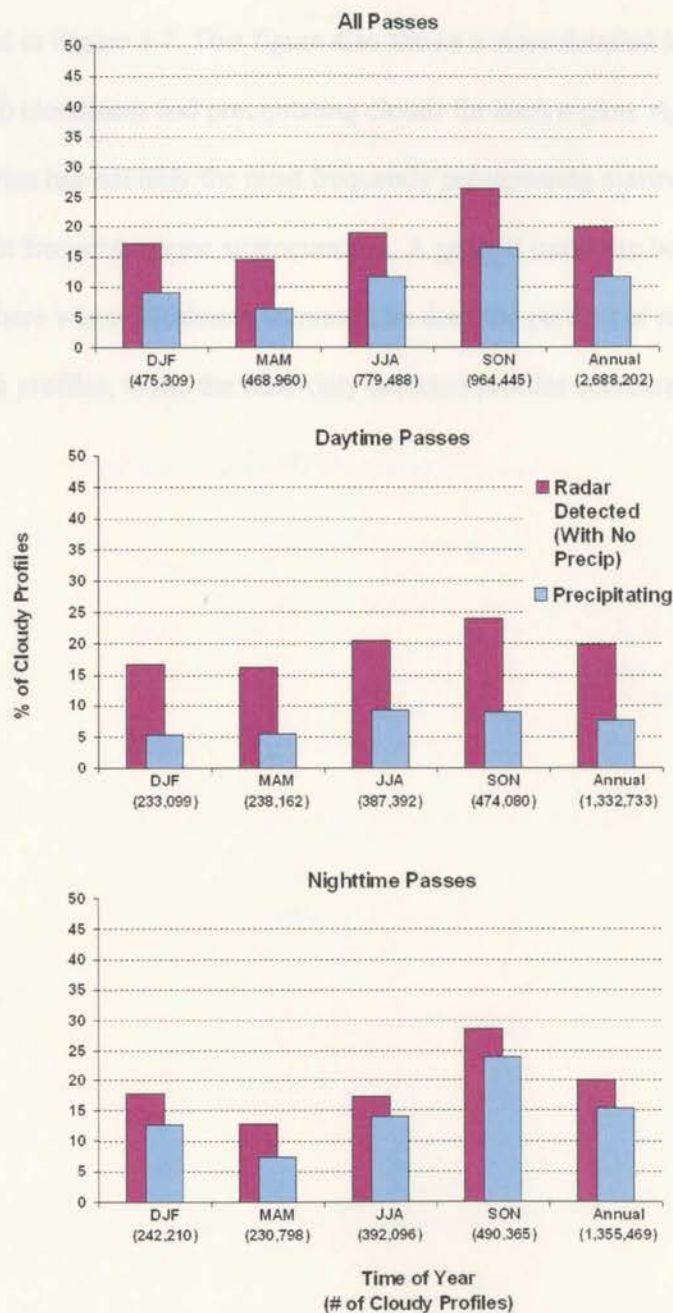further divided into all satellite passes, daytime passes, and nighttime passes*

46

S. America: Detection Frequency

All Passes

Daytime Passes

Nighttime Passes

Time of Year
(# of Cloudy Profiles)
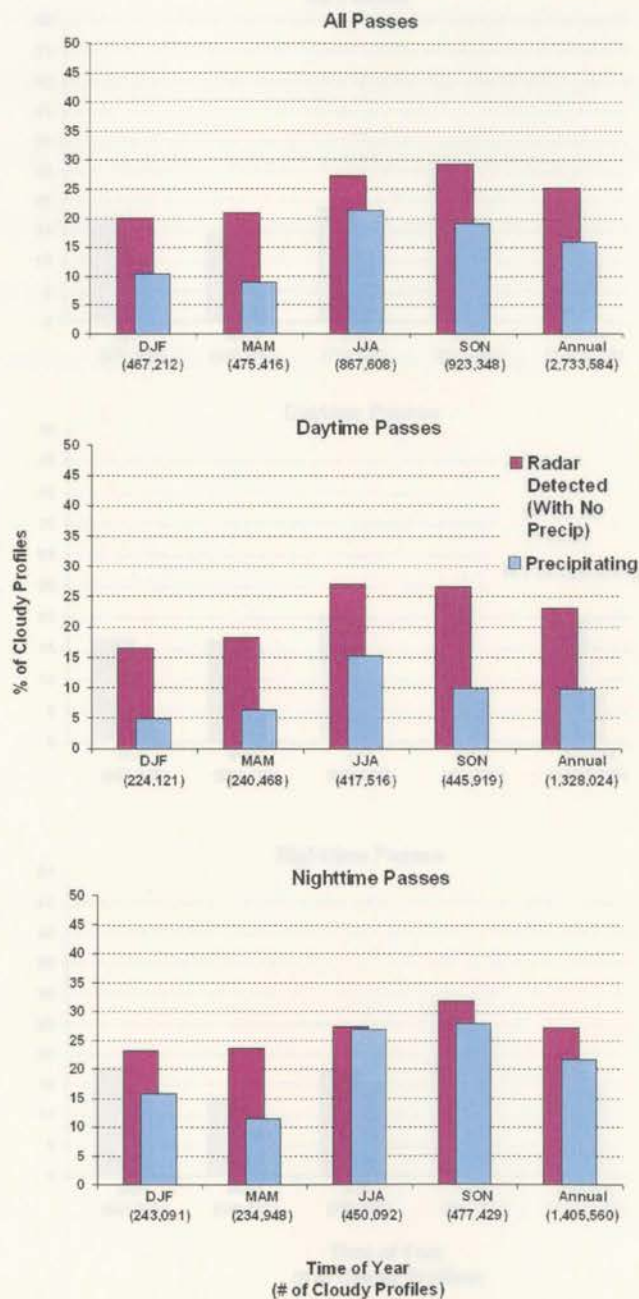
Figure 4.5 - The percentage of profiles over the South American region that are precipitating or radar-detected without precipitation for seasonal and annual averages, further divided into all satellite passes, daytime passes, and nighttime passes

47

Figure 4.6 - The percentage of profiles over the African region that are precipitating or radar-detected without precipitation for seasonal and annual averages, further divided into all satellite passes, daytime passes, and nighttime passes

48

Further insight into which sensors detect the marine stratocumulus throughout the year is found in Figure 4.7. This figure also shows a more detailed look into the seasonal cycle of both cloudiness and precipitating clouds for each region. Again it is clear that South America has not only the most frequently precipitating marine stratocumulus, but also the most frequent marine stratocumulus. A general trend can be found in all locations where when cloudiness increases, so does the percent of radar-detected and precipitating profiles, while the lidar-only detected profiles decrease.
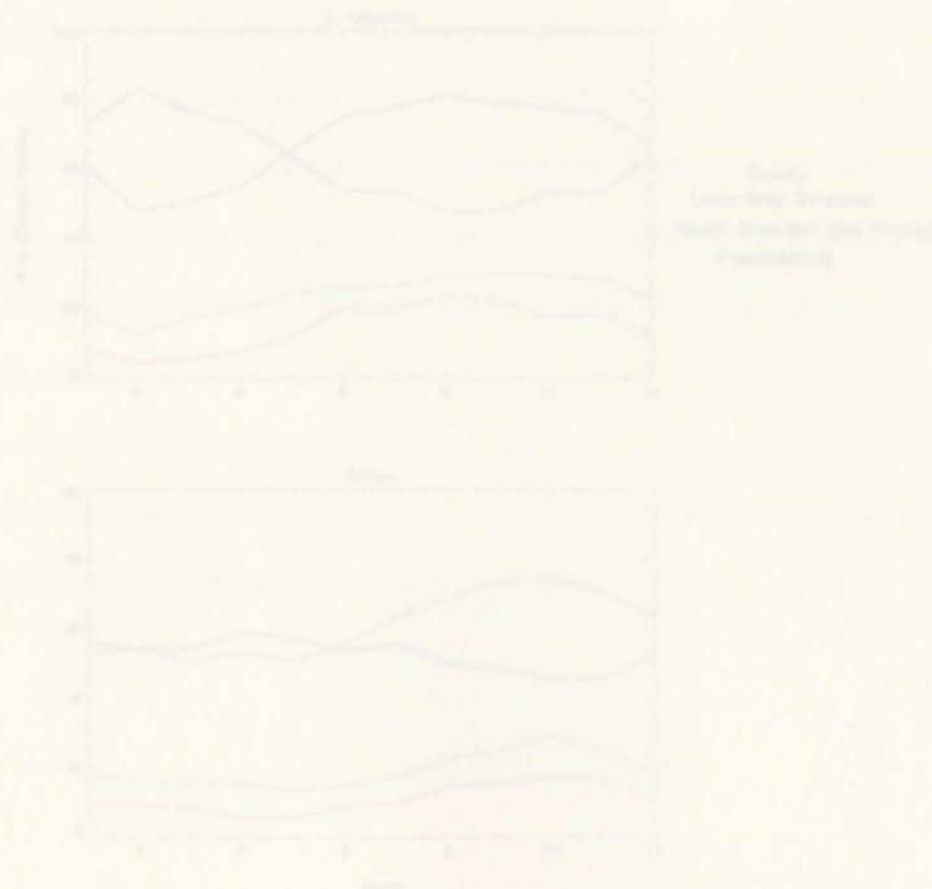
Figure 4.7 – The monthly percentages of clouds, rain, and radar or lidar-sensed profiles for each location (Note: the sum of the three colored lines is equal to 100% of the profiles)

Figure 4.7 - The monthly percentages of cloudy, rainy, and radar or lidar-detected profiles for each location (Note: the sum of the three colored lines is equal to 100% of the profiles)

4.2   Cloud and Precipitation Distribution Maps

4.2.1 Cloud Amount

An essential step toward observing the characteristics of marine stratocumulus is to find out where they are located. Annual averages of cloud amount detected by the radar and lidar for each location are shown in Figure 4.8. Annual average cloud amount is further separated into the daytime and nighttime passes in Figure 4.9. These figures show that South America has the highest overall frequency for marine stratocumulus, with Africa coming in a close second. Clouds in all three locations tend to have a maxima just offshore with somewhat of a northwest to southeast orientation. Regions that are further away from shore tend to have less stratocumulus amounts. The cloudiest location out of all three regions is in the South American region and can be covered by marine stratocumulus for about 90% of the A-train passes in a year. While no spatial differences appear between the daytime and nighttime passes, the nighttime passes have a larger overall frequency of marine stratocumulus presence.
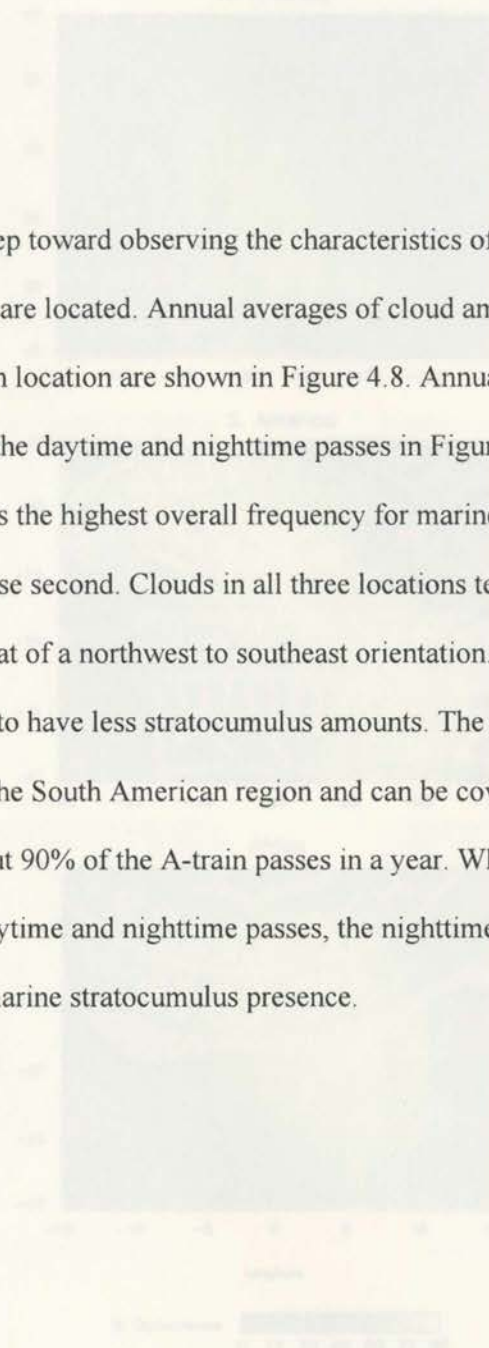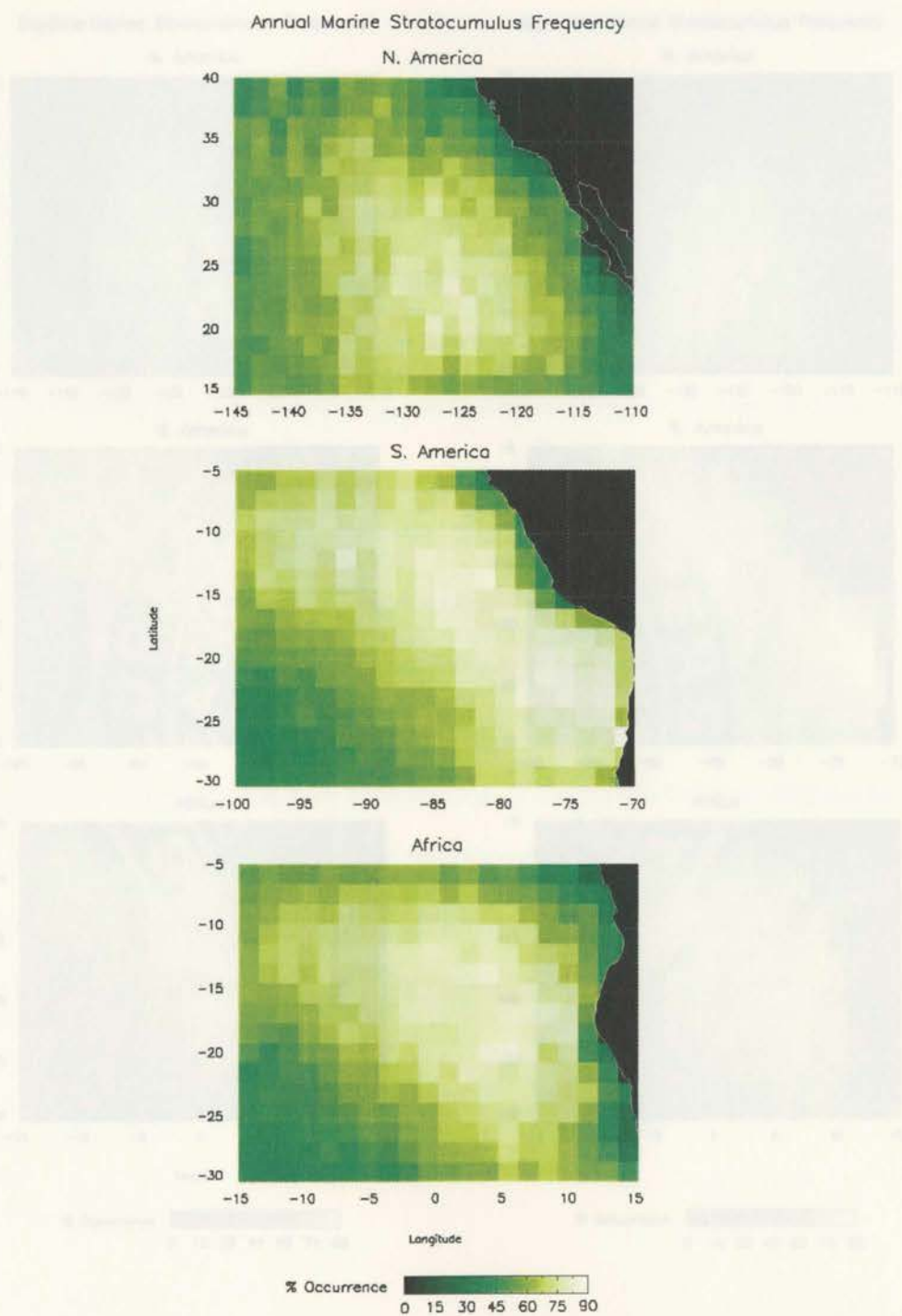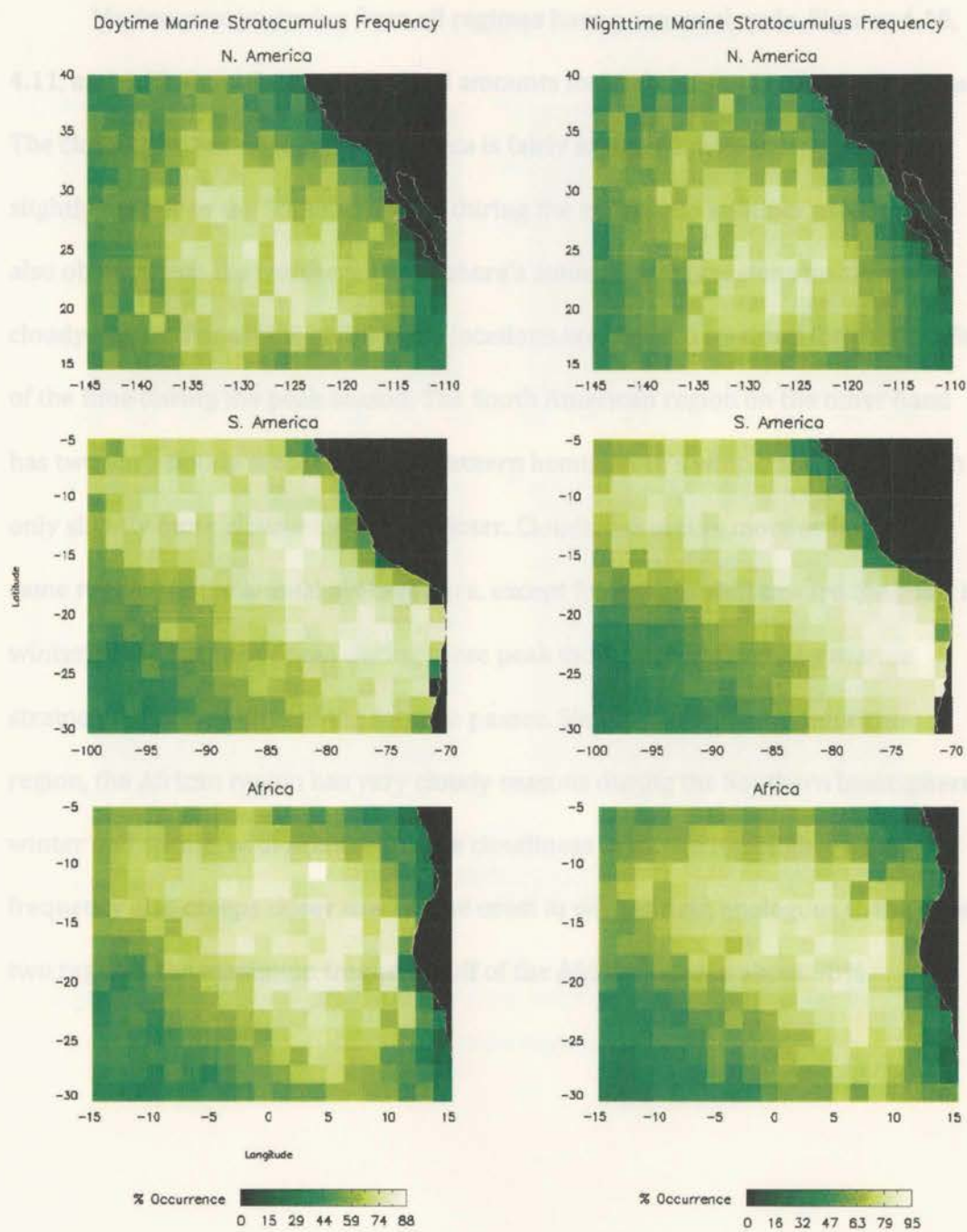
Figure 4.8 - *Annual averages of marine stratocumulus frequency for all passes at each location*
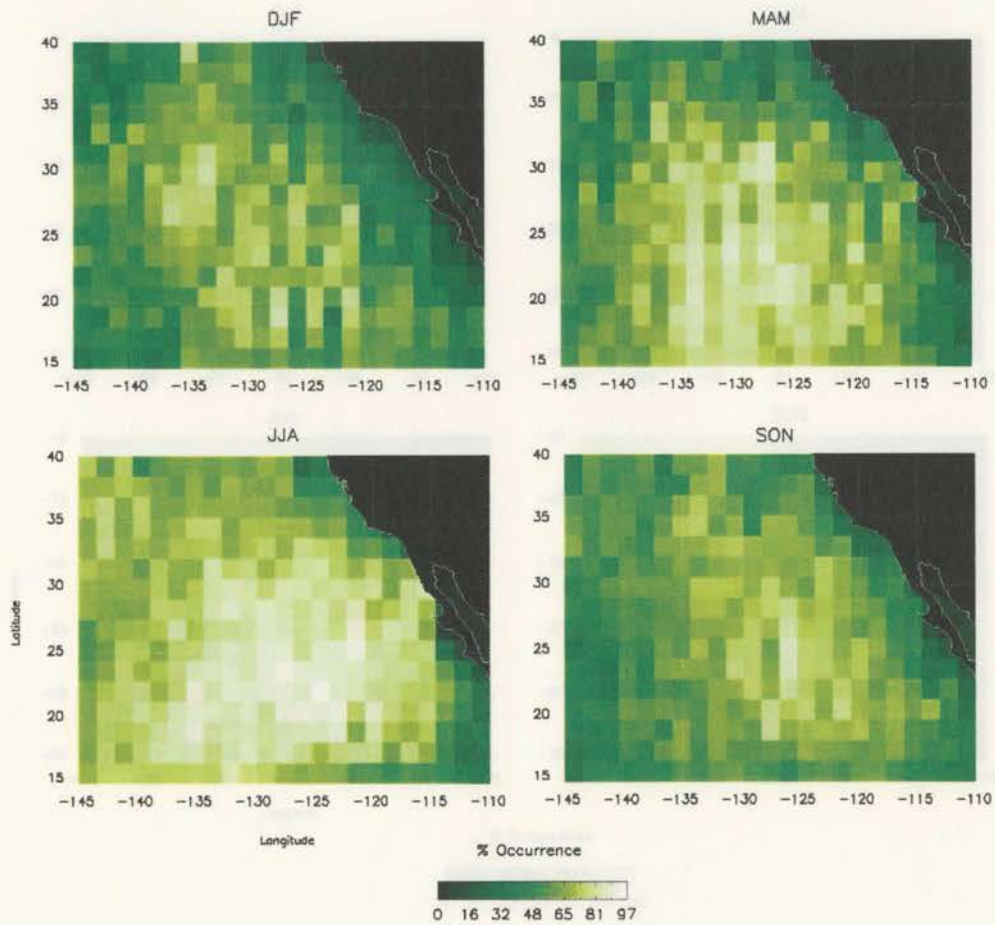
Figure 4.9 - *Annual averages of marine stratocumulus frequency for daytime and nighttime passes at each location*

Marine stratocumulus from all regimes have a seasonal cycle. Figures 4.10, 4.11, and 4.12 show the average cloud amounts for each season in all three regions. The cloud distribution in North America is fairly scattered, with clouds spreading slightly further to the South and West during the spring and summer months. It is also obvious that the Northern hemisphere's summer is this regions maximum cloudy season. Far off the coast, some locations are covered by cloud for about 97% of the time during the peak season. The South American region on the other hand has two very cloudy seasons in the Southern hemisphere's winter and spring, with only slightly more cloudiness in the winter. Cloudiness occurs more or less in the same regions as the annual average here, except for a slight shift toward the coast in winter. A wide area of ocean during these peak months are covered by marine stratocumulus for 100% of the satellite passes. Similar to the South American region, the African region has very cloudy seasons during the Southern hemisphere winter and spring, with relatively more cloudiness in the spring. Higher cloud frequency also creeps closer toward the coast in winter. And, analogous to the other two regions, the maximum frequency off of the African coast is about 98%.
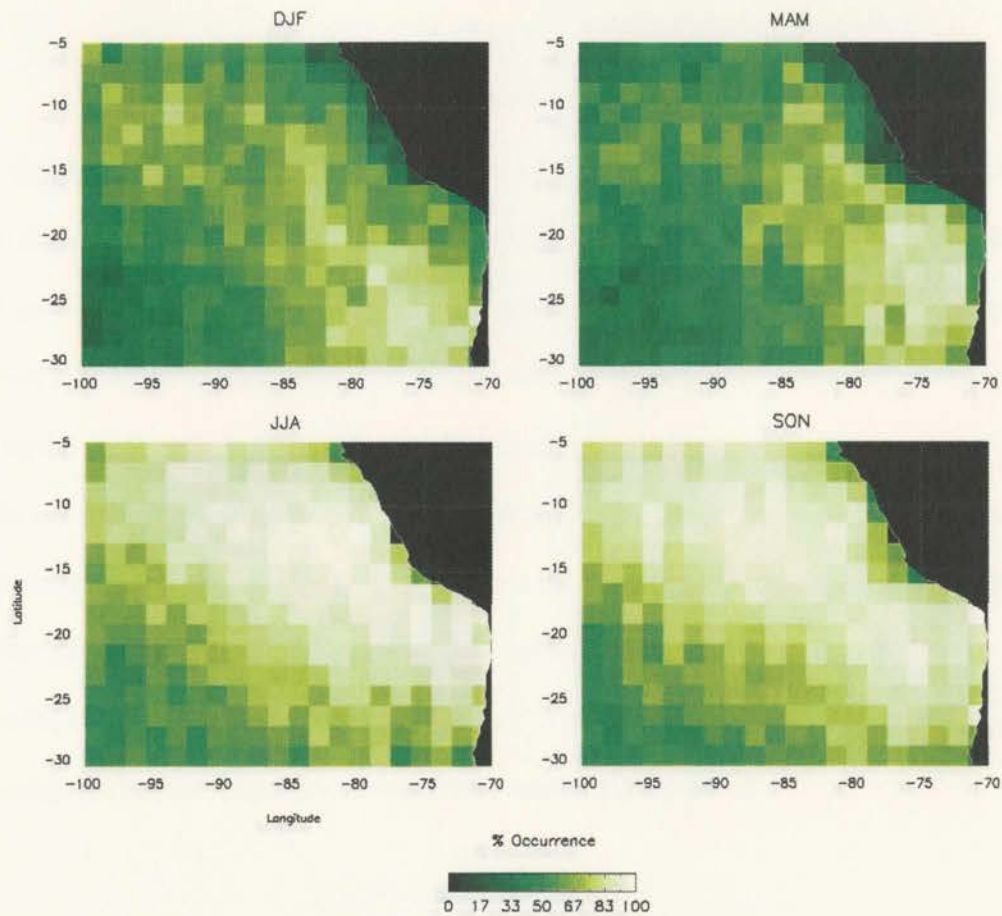
N. America: Seasonal Marine Stratocumulus Frequency

Figure 4.10 - *Seasonal averages of marine stratocumulus frequency for the North American region*
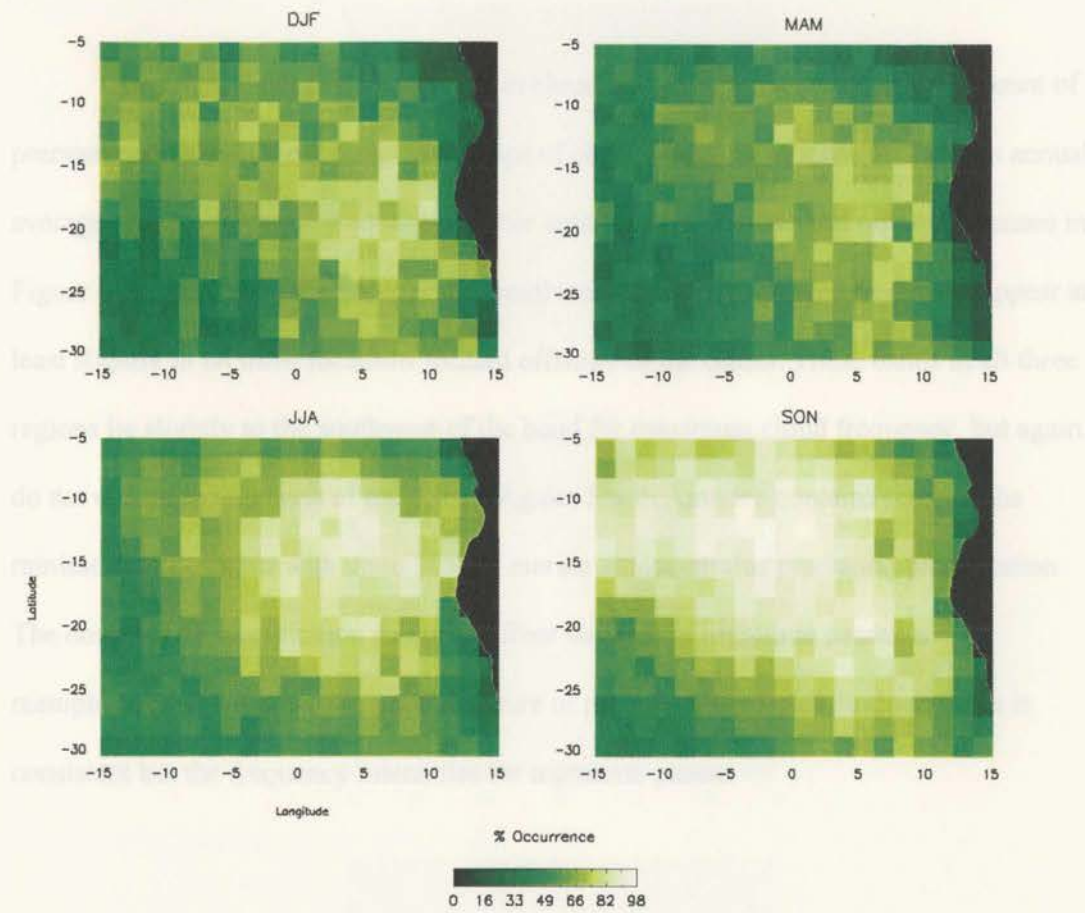
S. America: Seasonal Marine Stratocumulus Frequency

DJF   MAM

JJA   SON

% Occurrence

0 17 33 50 67 83 100

Figure 4.11 - Seasonal averages of marine stratocumulus frequency for the South American region
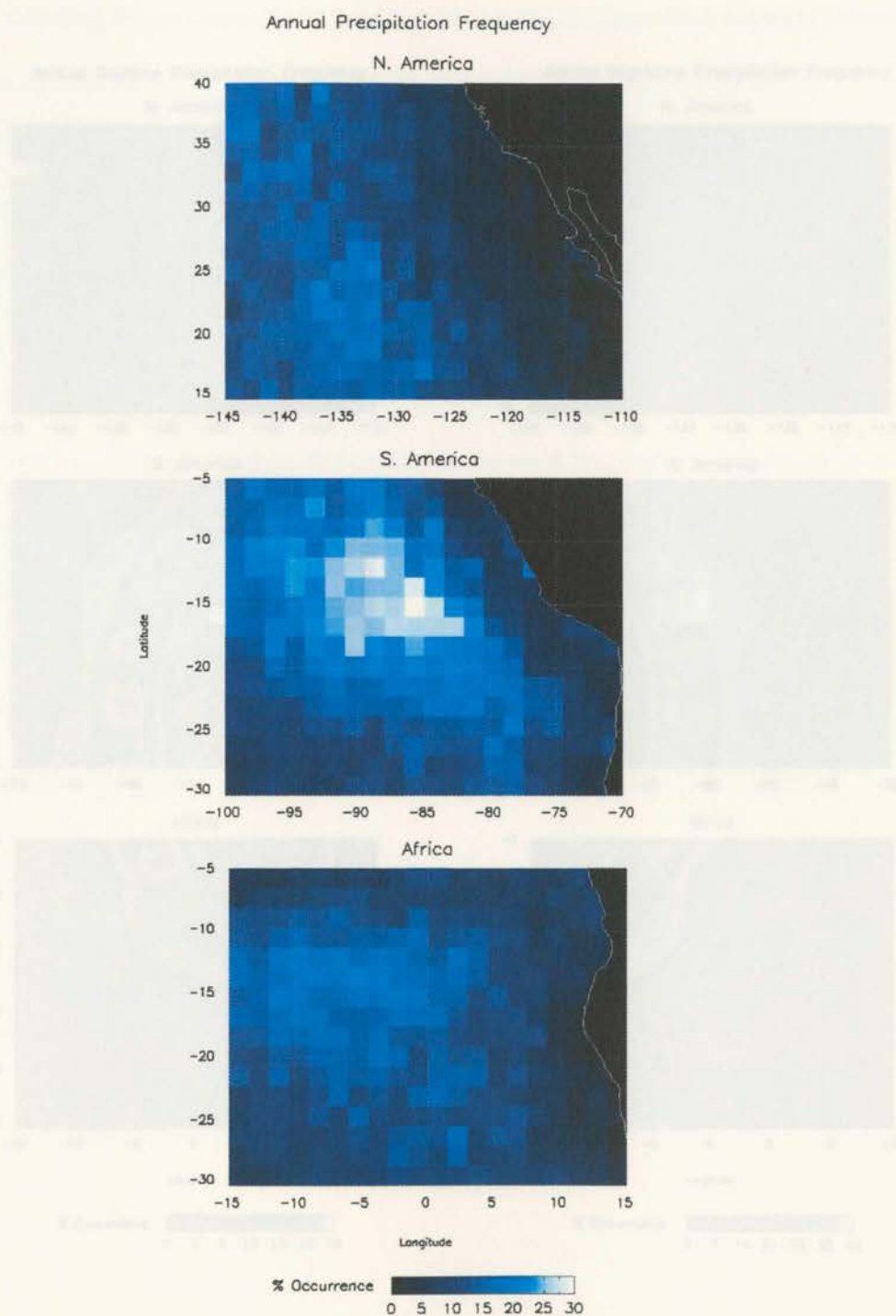
Africa: Seasonal Marine Stratocumulus Frequency

Figure 4.12 - *Seasonal averages of marine stratocumulus frequency for the African*

region

4.2.2 Precipitation Amount

One might think that an increase in cloud coverage would increase the amount of precipitation as well. Following from maps of cloud frequency, Figure 4.13 shows annual averages for precipitation frequency further split into the daytime and nighttime passes in Figure 4.14. Similarly, the northwest to southwest bands of increased frequency appear at least slightly in all three locations located offshore of the coasts. These bands in all three regions lie slightly to the southwest of the band for maximum cloud frequency, but again do not extend too far west of the coasts. Again, South America contains some of the rainiest stratocumulus with up to 30% of marine stratocumulus producing precipitation. The doubling of precipitation frequency from daytime to nighttime passes is reemphasized in Figure 4.14 as the structure of precipitating marine stratocumulus is consistent but the frequency intensifies for nighttime passes.
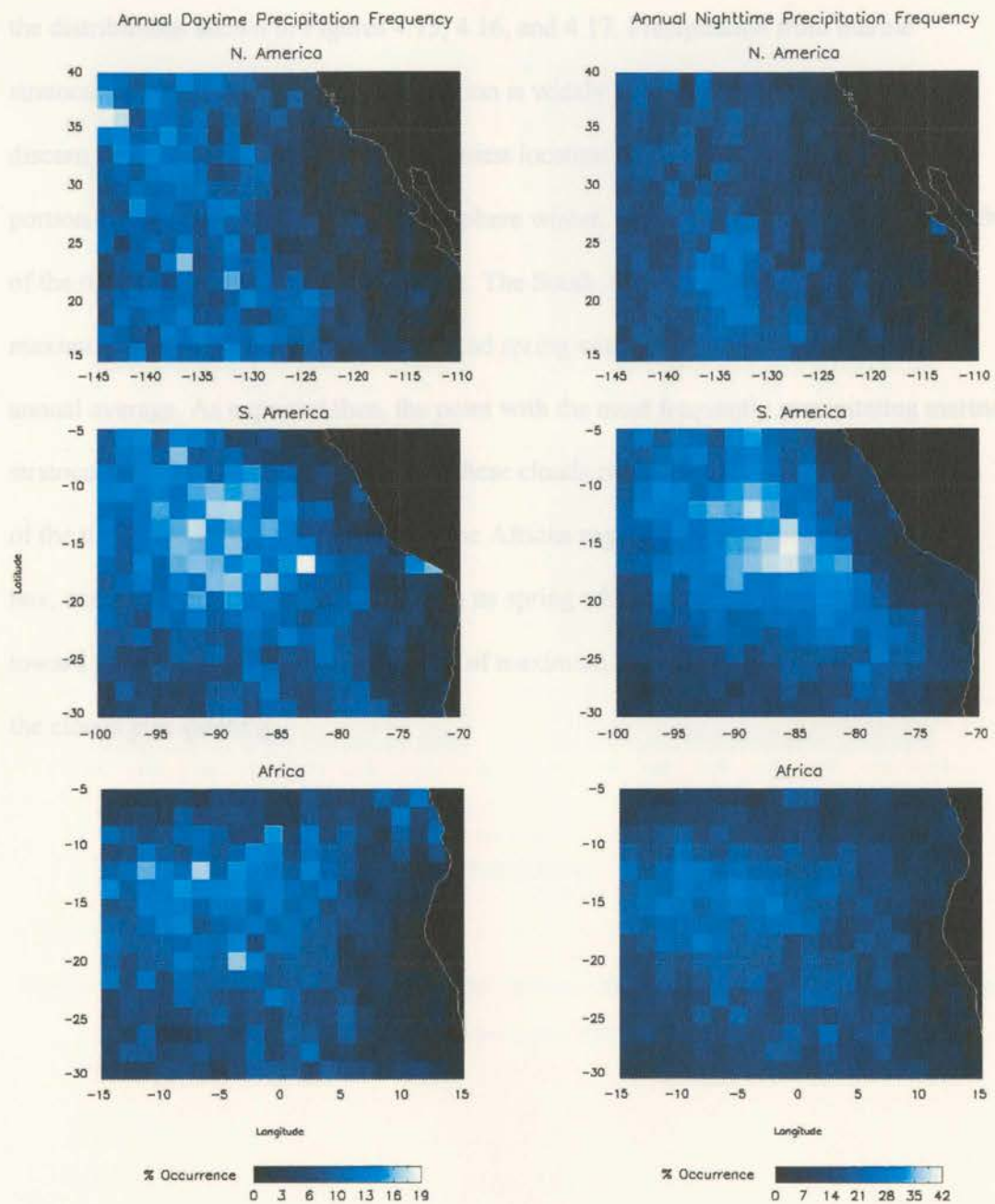
Annual Precipitation Frequency

Figure 4.13 – *Annual averages of marine stratocumulus precipitation frequency for all passes at each location*
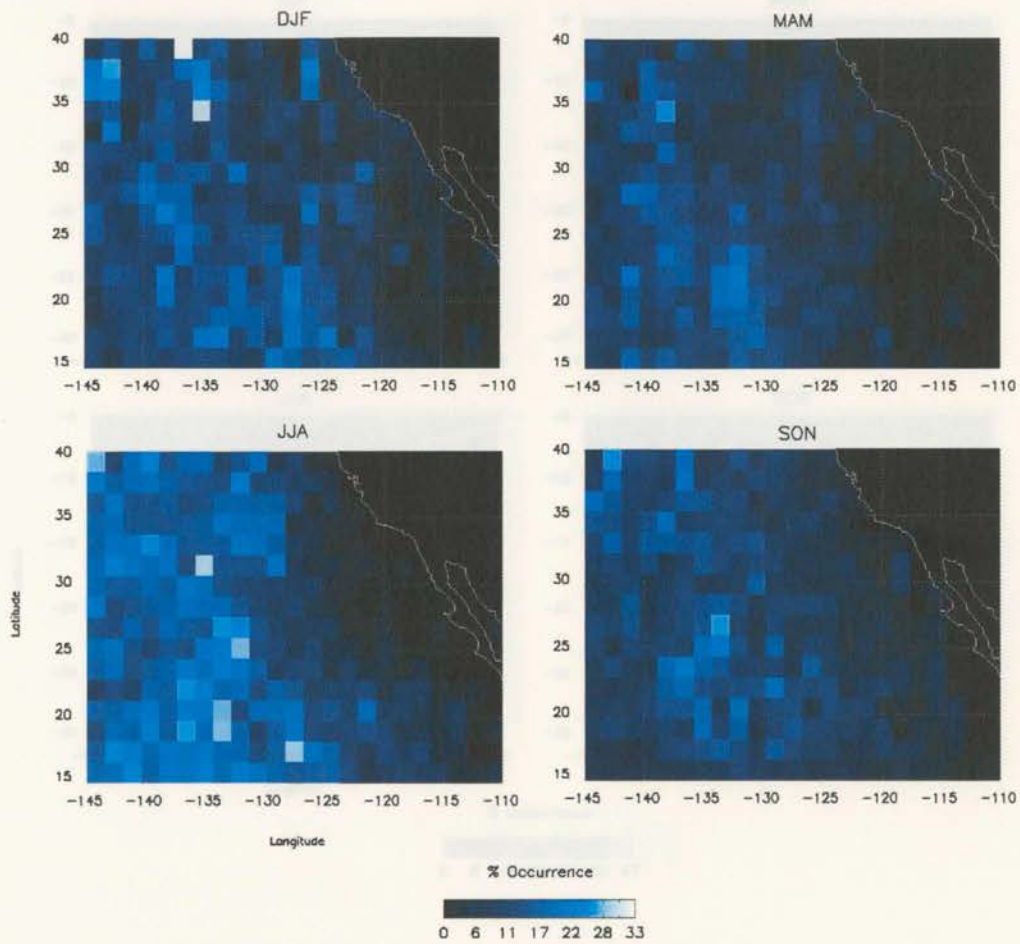
Figure 4.14 - *Annual averages of marine stratocumulus precipitation frequency for daytime and nighttime passes at each location*

Dividing the precipitation frequency into seasons for these three regions produces the distributions shown in Figures 4.15, 4.16, and 4.17. Precipitation from marine stratocumulus in the North American region is widely scattered and it is difficult to discern any type of organization. The rainiest location here occurs in the northernmost portion of the grid in the Northern hemisphere winter, and shows precipitation about 33% of the time that stratocumulus are present. The South American region again has its maximum frequencies during its winter and spring with a similar organization to the annual average. As expected then, the point with the most frequently precipitating marine stratocumulus occurs in the winter with these clouds producing precipitation about 47% of the time. And lastly, precipitation in the African region is mostly centered in the grid box, except for during the peak season in its spring where the precipitation is shifted far toward the west. It is here where regions of maximum precipitation occur with 35% of the clouds precipitating.

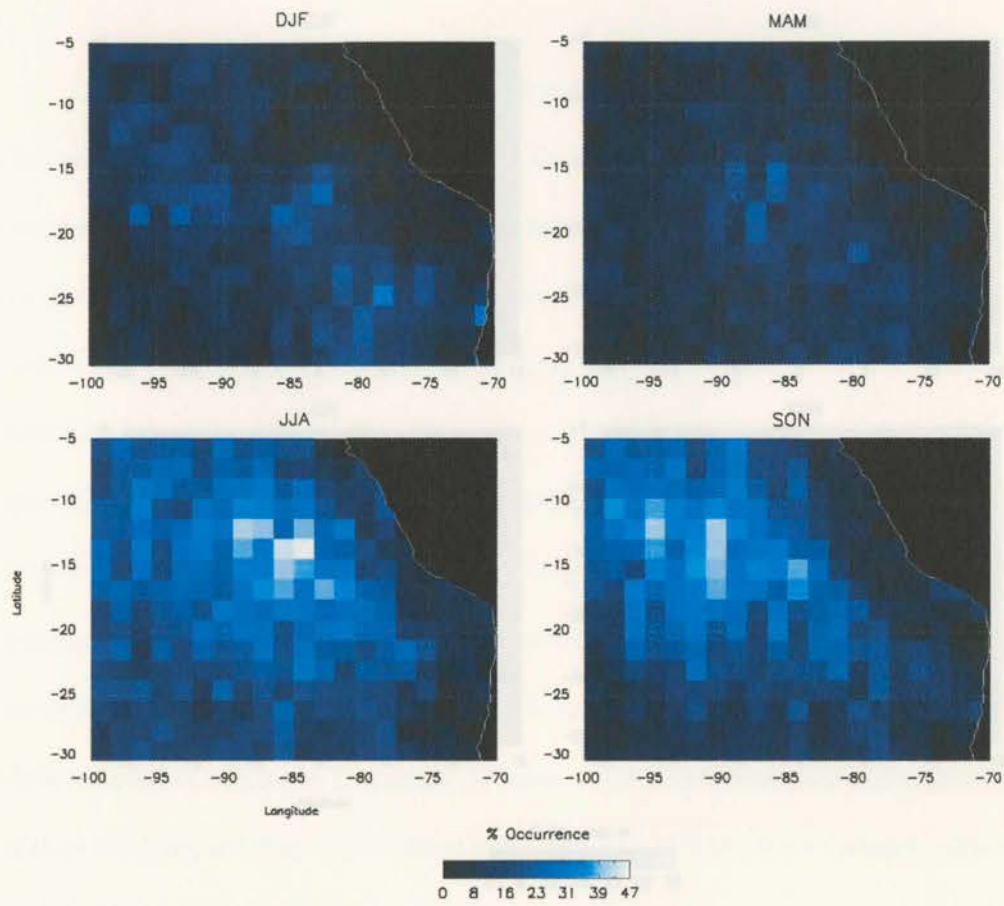*Figure 4.15 - Seasonal averages of marine stratocumulus precipitation frequency for the North American region.*

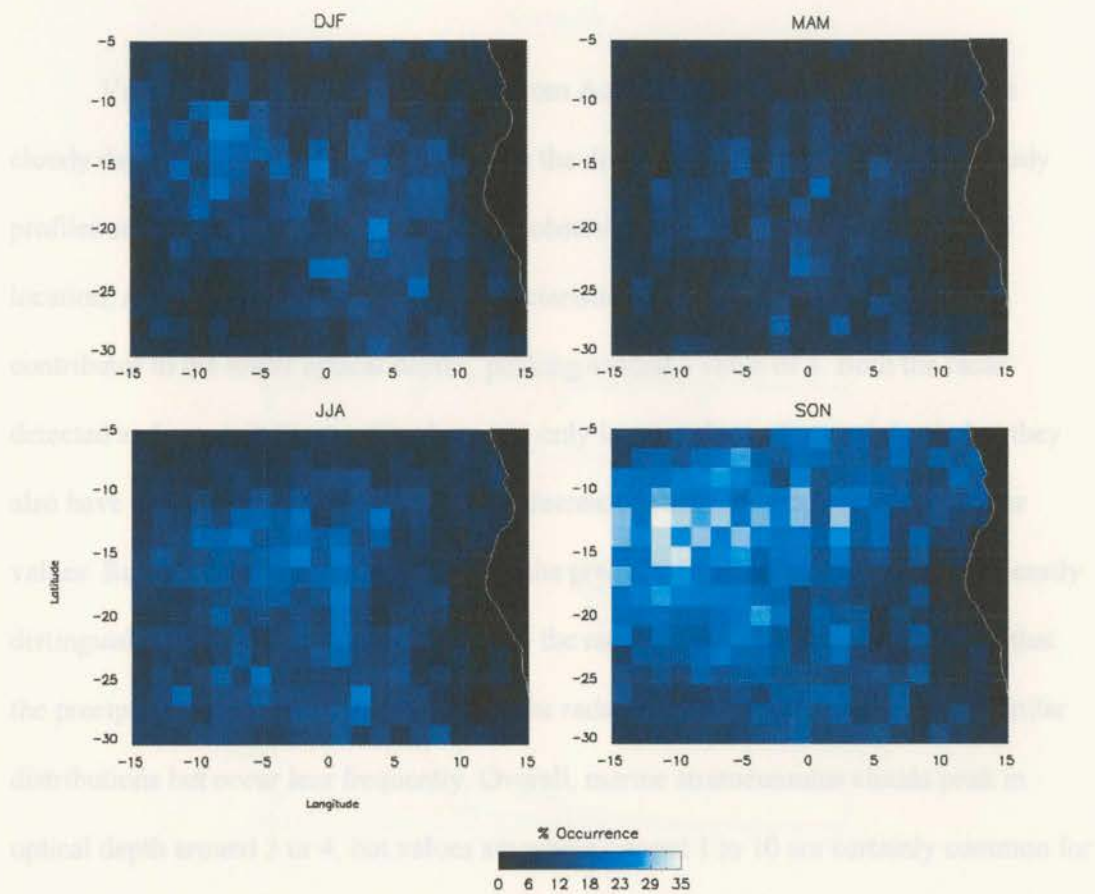**Figure 4.15** - *Seasonal averages of marine stratocumulus precipitation frequency for the North American region*

Figure 4.16 - Seasonal averages of marine stratocumulus precipitation frequency for the South American region

Figure 4.17 - Seasonal averages of marine stratocumulus precipitation frequency for the African region

4.3   Cloud Optical Depth

Values for optical depth retrieved from Aqua/MODIS were available for the

cloudy daytime profiles. Figure 4.18 shows the distribution of optical depth for cloudy

profiles sorted by their detection type. The observed properties hardly vary at all by

location, and so they all have similar characteristics. The lidar is clearly the biggest

contributor to the lower optical depths, peaking around a value of 3. Both the radar-

detected and precipitating profiles have not only larger values of optical depth, but they

also have a larger range with tail ends that decrease much more slowly than the lidar

values. Radar values peak around 6, while the precipitating curve does not have an easily

distinguishable peak, but is fairly similar to the radar curve. These images indicate that

the precipitating clouds are a subset of all the radar-detected clouds as they have similar

distributions but occur less frequently. Overall, marine stratocumulus clouds peak in

optical depth around 3 or 4, but values anywhere around 1 to 10 are certainly common for
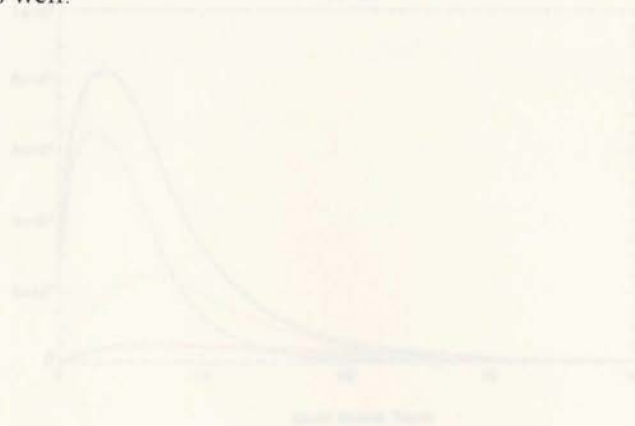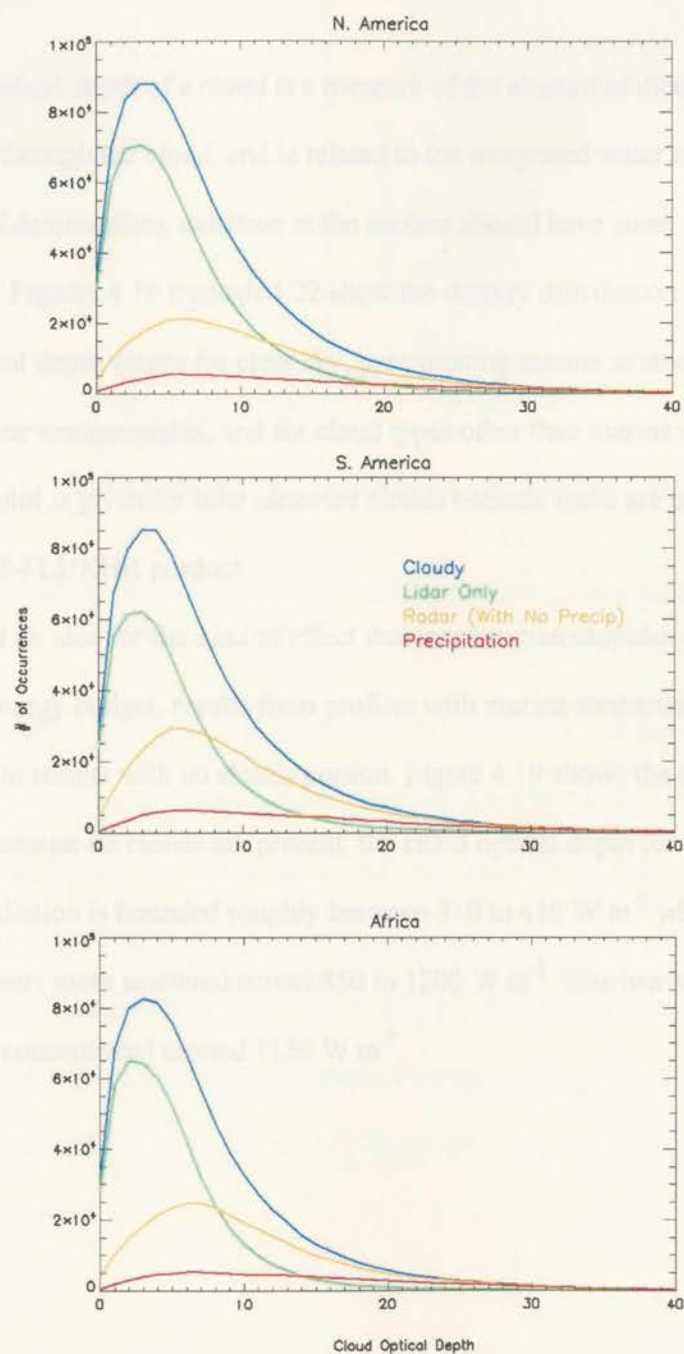
this cloud type as well.

Cloud Optical Depth Distribution

Figure 4.18 – *MODIS-retrieved cloud optical depth values sorted by the type of marine stratocumulus for each region*

4.4 Cloud Radiation Properties (Fluxes)

The optical depth of a cloud is a measure of the amount of direct-beam radiation that makes it through the cloud, and is related to the integrated water content. Therefore, the amount of downwelling radiation at the surface should have some correlation to the optical depth. Figures 4.19 through 4.22 show the density distribution of downwelling flux and optical depth values for clear sky, precipitating marine stratocumulus, radar-detected marine stratocumulus, and for cloud types other than marine stratocumulus. Note that no plot is given for lidar-detected clouds because these are not accounted for in the current 2B-FLUXHR product.

To get an idea for the kind of effect that marine stratocumulus and precipitation have on the energy budget, results from profiles with marine stratocumulus clouds must be compared to results with no clouds present. Figure 4.19 shows the distributions for clear skies. Because no clouds are present, the cloud optical depth for these profiles is 0. Longwave radiation is bounded roughly between 310 to 410 W m^{-2} while shortwave radiation appears more scattered across 850 to 1200 W m^{-2}. Shortwave flux values are most heavily concentrated around 1150 W m^{-2}.
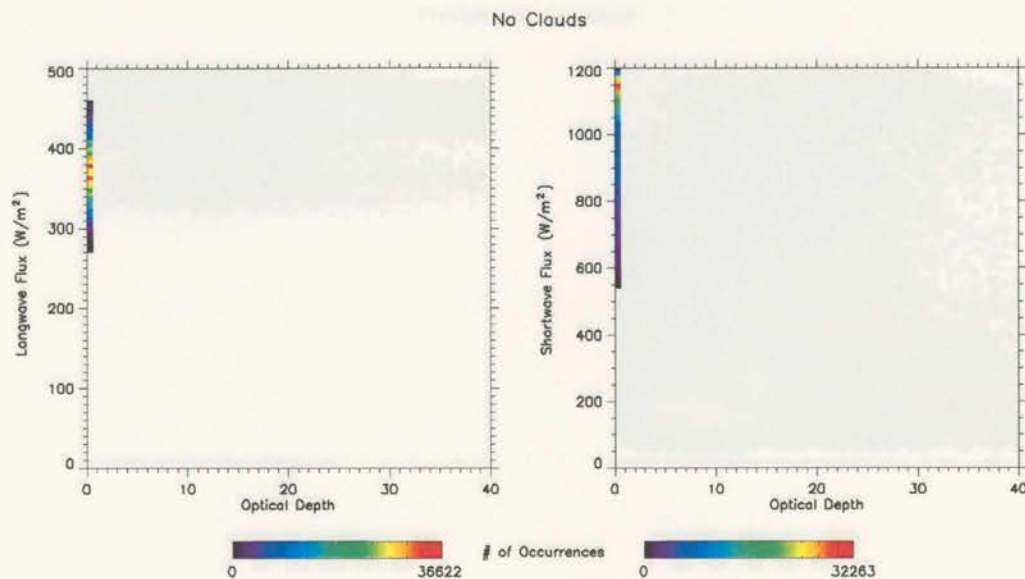
Figure 4.19 - *Flux values vs. optical depth when no clouds are present*

Precipitating marine stratocumulus are optically thick and drive the amount of longwave radiation toward higher values, spanning from about 400 to 500 W m^{-2} as shown in Figure 4.20. Both the longwave and shortwave fluxes occur over a relatively wider range of optical depth values, ranging from about 1 to 40 with the maximum frequency occurring for optical depths around 6 or 7. Shortwave fluxes are much more varied than longwave fluxes for the instance of a precipitating cloud. Values at the surface range from about 50 to 450 W m^{-2}. These are the lowest shortwave flux values out of all of the plots.
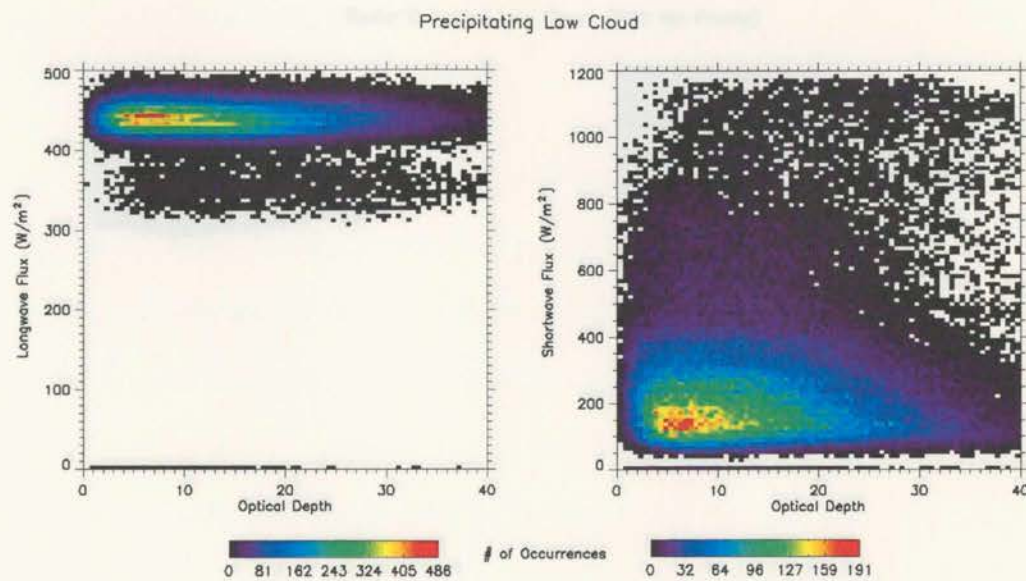
Figure 4.20 - *Flux values vs. optical depth when marine stratocumulus are precipitating*

For the radar-detected clouds presented in Figure 4.21, a maximum frequency of the distribution occurs for the same longwave flux values, around 400 to 500 W m^{-2}, only this time a secondary maximum also occurs between 300 to 400 W m^{-2}. One important difference from the precipitating fluxes is that the optical depths are limited to a range similar to the clear sky scenario, normally falling between 1 and 20, with a maximum occurrence around 6. The shortwave fluxes for radar-detected clouds vary greatly as values extend all the way from 100 to 1200 W m^{-2} with the most frequent values between 200 and 600 W m^{-2}.

69

Radar Detected Low Cloud (With No Precip)
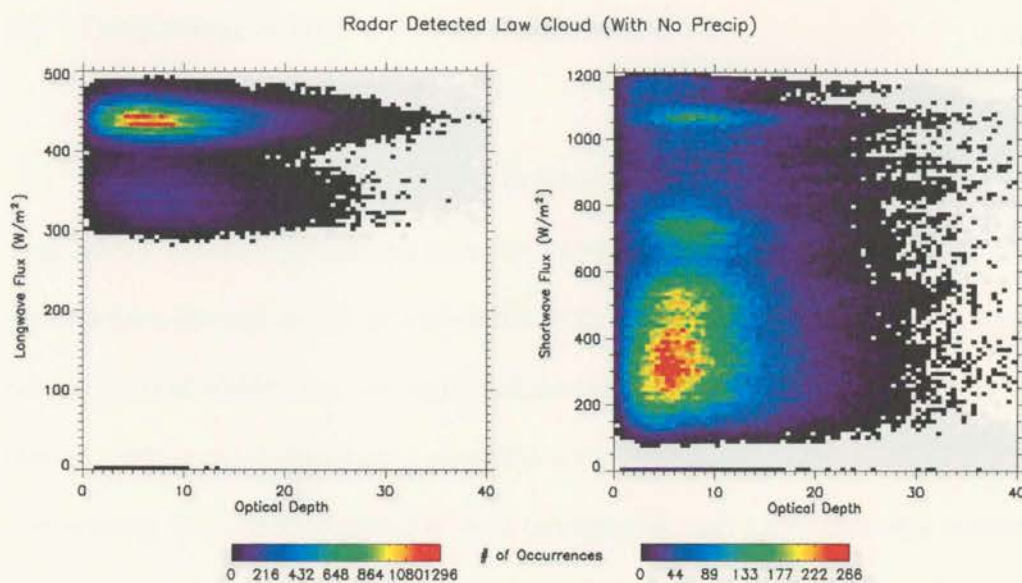
Figure 4.21 - *Flux values vs. optical depth when the radar detects the marine stratocumulus but no precipitation is present*

To see how the effects of marine stratocumulus differ from the effects that other cloud types have on the radiation budget, Figure 4.22 shows the results for any cloud defined by the 2B-GEOPROF-LIDAR product that is not considered to be marine stratocumulus. This image shows a nice correlation between the fluxes and the optical depth. As the clouds increase the amount of longwave radiation at the surface, the optical depth values increase as well, representative of overall thickening of the clouds. Similarly, the greater amounts of extinguished shortwave radiation at the surface corresponds to greater optical depths. Compared to the cases with marine stratocumulus clouds, the fluxes seem to fall within similar ranges. However, cases with marine stratocumulus clouds tend to have larger overall optical depth values.
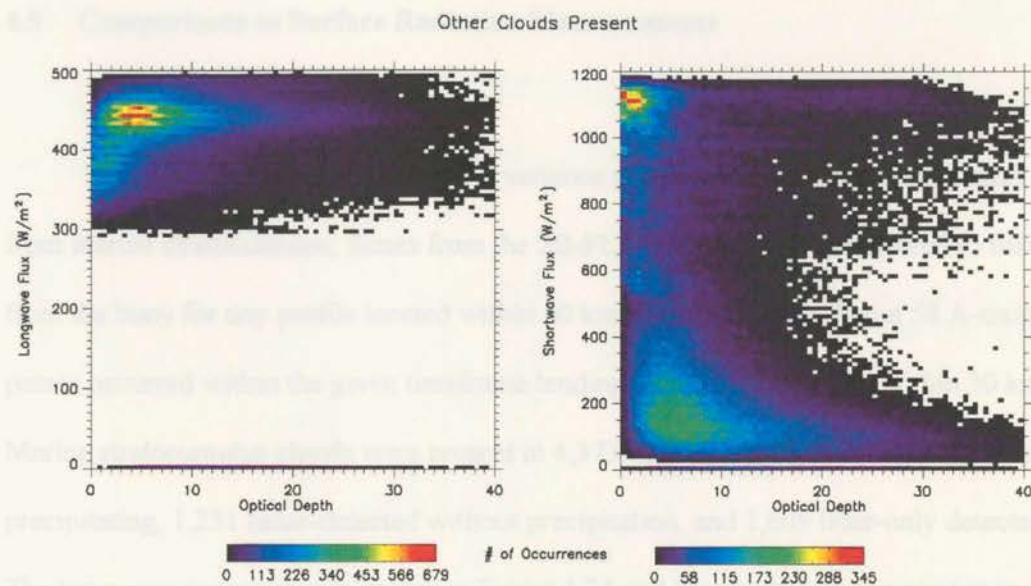
Figure 4.22 - Flux values vs. optical depth for cloud types other than marine stratocumulus

By comparing the marine stratocumulus plots with the clear sky plot, it becomes apparent that marine stratocumulus increase the amount of downwelling longwave radiation from the typical 310 to 410 W m⁻² range up to about 500 W m⁻². These clouds also decrease the amount of incoming shortwave radiation bringing it to as low as 50 W m⁻², especially if precipitation is present. One more effect of precipitation is the increase in range of optical depth, as precipitating marine stratocumulus have thicker values than clear skies, non-precipitating stratocumulus, or other cloud types.

71

4.5   Comparisons to Surface Radiation Measurements

In order to further understand the variance of longwave and shortwave fluxes from marine stratocumulus, fluxes from the 2B-FLXHR product are compared to fluxes from the buoy for any profile located within 30 km of the buoy site. About 58 A-train passes occurred within the given timeframe lending about 5,277 profiles within 30 km. Marine stratocumulus clouds were present in 4,373 of these profiles, 744 of which were precipitating, 1,231 radar-detected without precipitation, and 1,609 lidar-only detected. The longwave comparison is shown in Figure 4.23 and the shortwave comparison in Figure 4.24. Before the results are discussed, it is worth noting that these plots show no changes when organized by distance from the buoy, and so results from any distance to the buoy should have equal weighting.
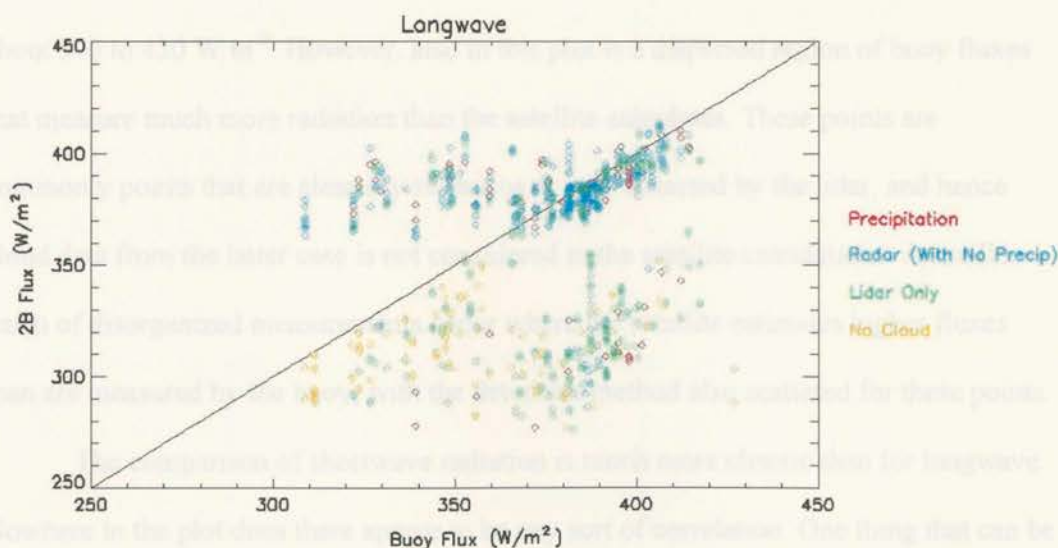
Figure 4.23 - *Longwave flux values compared between the buoy and 2B-FLXHR product for different types of marine stratocumulus*
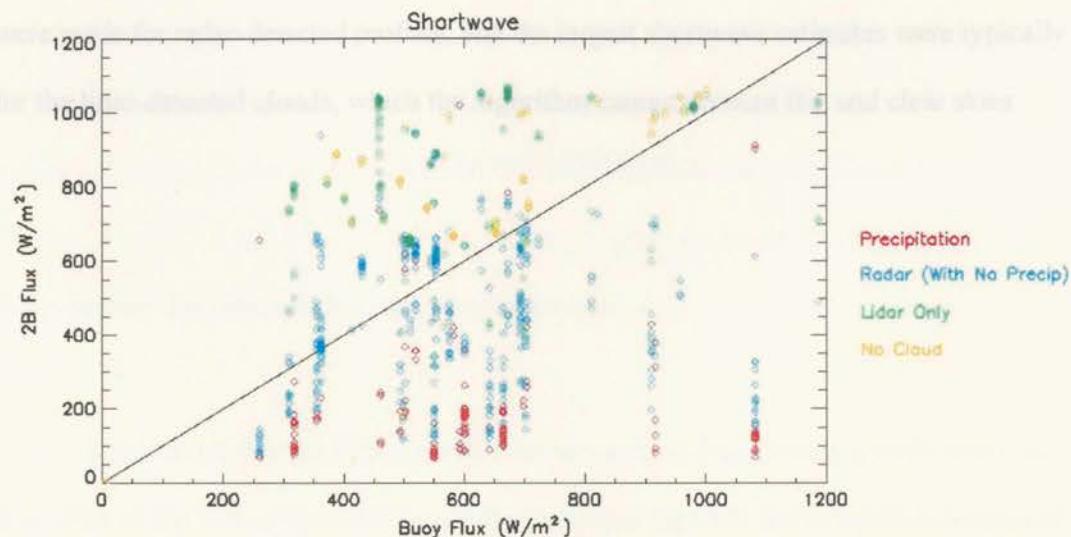
Figure 4.24 - *Shortwave flux values compared between the buoy and 2B-FLXHR product for different types of marine stratocumulus*

Comparisons of the longwave fluxes show somewhat of a 1:1 correlation between about 370 to 420 W m^{-2}. However, also in this plot is a dispersed region of buoy fluxes that measure much more radiation than the satellite calculates. These points are commonly points that are clear sky scenarios or only detected by the lidar, and hence cloud data from the latter case is not considered in the satellite calculations. A smaller patch of disorganized measurements occur where the satellite estimates higher fluxes than are measured by the buoy, with the detection method also scattered for these points.

The comparison of shortwave radiation is much more chaotic than for longwave. Nowhere in the plot does there appear to be any sort of correlation. One thing that can be seen from this plot though is the layering of detection types based on the satellite flux calculations. Independent of the buoy measured flux, the satellite estimated much lower

values for shortwave radiation in the presence of precipitation. Slightly higher estimates were made for radar-detected profiles, and the largest shortwave estimates were typically for the lidar-detected clouds, which the algorithm cannot account for, and clear skies.

5. CONCLUSIONS

5.1 Sensor Detection of Marine Stratocumulus

The characteristics of the sensors used throughout this research greatly affect the data. One of the first conclusions established was that the CPR did in fact detect some of the non-precipitating marine stratocumulus. Even though only 12% of marine stratocumulus clouds produced precipitation, about 30-35% of the marine stratocumulus were detected by the radar. Of these radar-detected clouds, 36% produced precipitation. This is an important result because it shows that CloudSat detects more than just precipitation in the lowest layers of the atmosphere. CPR returns are directly related to the size of the hydrometeors being detected. Therefore, if CloudSat detects a portion of non-precipitating low level cloud, it is because the cloud drop sizes are large enough for the CPR to see yet small enough to be suspended as a cloud droplet and not fall as a drizzle droplet.

Droplets of precipitation are larger than cloud droplets, and so this would explain why the precipitating profiles are a subset of the radar-detected profiles. As cloudiness increased for a region, the radar-detected and precipitating profiles also increased, possibly due to thickening of the clouds, which would increase the droplet sizes and reduce the number of lidar-only detected clouds. Instances where the radar did not detect

a precipitating profile could be due to flaws in the method of classifying marine

stratocumulus where it is possible for clouds above 5 km to exist over low level clouds.

While the CPR provides crucial information about the precipitation in marine

stratocumulus, the lidar makes it possible to detect the stratocumulus in the first place.

Without the lidar about 60-65% of the marine stratocumulus would not have been

detected.

5.2 Cloud and Precipitation Frequency

The maps and plots for the three locations of marine stratocumulus produce key

climatologies for these clouds. All results show South America as one of the cloudiest

marine stratocumulus regions and also with the most frequently precipitating

stratocumulus. South America's peak season for marine stratocumulus and precipitating

marine stratocumulus occurs during its winter and spring months. Peak cloudiness also

occurs in the Southern hemisphere spring for the African region and the Northern

hemisphere summer for the North American region. The months of March, April, and

May appear to have reduced marine stratocumulus activity for all locations. And lastly,

even though the frequency of precipitation in marine stratocumulus seem to be correlated

spatially and temporally to the location of the frequency of marine stratocumulus cloud

cover, this is not always the case as some regions of maximum cloudiness do not contain

the most frequently precipitating marine stratocumulus. These findings largely agree with

similar climatologies, such as those produced by ISCCP, Klein and Hartmann (1993), and

Leon et al. (2008). Important differences between the results shown in Chapter 4 and these previous datasets is the increased spatial resolution and the duration of the study.

When split into the daytime and nighttime passes, the nighttime marine stratocumulus showed a clear sign of cloud thickening and increased precipitation. Overall, the precipitation frequency of marine stratocumulus doubled from the daytime to nighttime passes. It is important to note here that due to the limited passing times of the satellites, this result does not necessarily reveal a diurnal cycle, but instead represents more precipitation around the time of the nighttime passes.

Each of the subtropical locations have many similarities that make them favorable for marine stratocumulus, yet the results provided in Chapter 4 show evidence for a number of differences as well. Especially interesting is the temporal differences between the South American and African regions, which are located at the same latitudes in the same hemisphere.

What causes these seasonal and spatial changes in marine stratocumulus or precipitation cannot be answered using only the results discussed here. However, the maximum frequency of marine stratocumulus in all three regions occurs during the months where the subtropical high is at its peak strength for each of the locations. Klein and Hartmann (1993) state that the peak of the subtropical high produces steady subsidence and surface fluxes at a time when the surface fluxes are highest due to sea-air temperature differences, creating conditions favorable for marine stratocumulus formation. Some of the factors that could influence the location and seasonality of marine stratocumulus include oceanographic properties, the strength of the subtropical high, the influence of different air masses, or a number of other characteristics. Reasons for why

the drizzle occurs where it does and when could also have something to do with different types of air masses over the three locations during different times. For example, biomass burning increases the amount of aerosols in the atmosphere, and is known to have a seasonal cycle in all three locations.

5.3 Radiative Properties

Contributions from the MODIS optical depth were helpful to characterize the long term averages for this parameter. With typical values between 1-10 for marine stratocumulus, the radar detects the larger end of the spectrum with only the lidar detecting most of the clouds with optical depths below 5. More specifically, precipitating profiles are the largest contributor to optical depths above 20. Both precipitating and non-precipitating marine stratocumulus tend to have increased values of cloud optical depth compared with other cloud types, proving just how influential these clouds are to the radiation budget.

Results from the 2B-FLXHR product helped to quantify the typical effects that the radar-detected marine stratocumulus have on the downwelling surface radiation. As expected, precipitating marine stratocumulus increase the longwave radiation and decreased the shortwave radiation reaching the surface. Keeping in mind that the fluxes for precipitating profiles have increased uncertainty, the longwave fluxes were increased by 100 W m^{-2} even though some cases increased the longwave radiation by as much as 150 W m^{-2}. These effects are particularly important because of the role that longwave radiation plays on the cloud microphysical scale and its role in global climate.

Shortwave fluxes generally decreased by 900 W m^{-2} in the presence of marine stratocumulus clouds, but this number typically varied between 800 to 1000 W m^{-2}. The influence of marine stratocumulus detected by the CPR that are not precipitating appears to be a mix of the characteristics between the precipitating marine stratocumulus and clear sky. This is because many of the radar-detected profiles will have some sections of the cloud detected by the lidar, which will produce clear sky signals from the 2B-FLUXHR product. For the profiles that do not resemble clear sky signals, the distribution reflects that of the lower intensity precipitating profiles. A better understanding of the amount of shortwave radiation reaching the surface in marine stratocumulus is important because of increased knowledge about the surface fluxes between the ocean and the atmosphere, which affects both the upper ocean and atmospheric boundary layer dynamics.

When compared to the surface observations from the buoy, the satellite calculated longwave fluxes appeared to agree on a number of the profiles. These profiles are the cases where the wealth of data from the A-train satellites can be matched or combined with the buoy location data. Many of the instances where the satellite calculated flux was lower than the buoy flux were from lidar-only or clear sky profiles. While the shortwave flux comparisons were very random, the satellite calculated fluxes still showed their trend of near clear sky values for the lidar-only detected profiles, some decreased radiation for the radar-detected profiles, and the most decreased radiation for the precipitating profiles.

The lack of correlation here is most likely due to the satellite algorithm being extremely sensitive to cloud properties for shortwave radiation. For both the longwave and the shortwave fluxes, comparisons with in situ data will always be further

complicated by the spatial variability of marine stratocumulus. While the closed cell marine stratocumulus tend to be more spatially homogenous, open cell convection can produce a localized region of heavy precipitation right beside clear skies. Because the A-train samples are never directly overhead of the buoy, this is a likely cause for many inconsistencies in the data.

5.4 Future Research

Despite the fact that new data is presented from this research, there is still much to learn about marine stratocumulus clouds. One option for expanding the use of these results would be to apply the same techniques to other known locations of frequent or non-frequent marine stratocumulus outside of the subtropical regions. Expanding the dataset past February 15, 2009 would also increase the amount of seasons and years being sampled, strengthening the dataset. Looking into the El Niño Southern Oscillation (ENSO) index for these periods would be an interesting task as well. The end of 2006 was a slight El Niño event while the end of 2007 and into 2008 was a slight La Niña period. Comparing the properties of the marine stratocumulus for these two instances would be a start to understanding ENSO's effect on this cloud type in different regions. Any one of these options would further increase the overall climatology for marine stratocumulus clouds.

Other properties of precipitating and non-precipitating marine stratocumulus can also be considered using CloudSat products. The precipitation rate from the 2C-COLUMN-PRECIP algorithm could be used to quantify the intensity of the precipitation.

Or, the maximum reflectivity in the radar-detected profiles could be examined and compared to precipitating and non-precipitating profiles. Boundary layer properties from the ECMWF-AUX product might also divulge information about the thermodynamics below both precipitating and non-precipitating clouds. All of these paths would provide further details into the microphysics and dynamics of marine stratocumulus.

Flux values for marine stratocumulus should also improve with the upcoming release of a new FLXHR product. This new product improves on the current version by including cloud and aerosol data from CALIPSO and enhancing the representation of cloud properties using MODIS cloud optical properties and CloudSat rainfall products.

Lastly, based on some of the scattered correlations between the fluxes from both the buoy and the satellite data, perhaps a time average of the buoy or spatial average of the satellite data might reduce the influence of the spatial heterogeneity. An option to sample closer to the buoy would be to use a MODIS product that is not collocated with the CloudSat track so that the closest pixel in the swath to the buoy can be obtained. For the fluxes that did match up, more of the satellite data can be combined to the buoy dataset in order to provide a more complete picture of the cloud field. For example, cloud fraction and other cloud layers could be considered to see their true effect on radiation at the surface.

REFERENCES

Ackerman, A. S., O. B. Toon, and P. V. Hobbs, 1993: Dissipation of marine stratiform clouds and collapse of the marine boundary layer due to the depletion of cloud condensation nuclei by clouds, *Science*, **262**, 226–228.

Ackerman, S., K. Strabala, P. Menzel, R. Frey, C. Moeller, L. Gumley, B. Baum, C. Schaaf, and G. Riggs, 1997: *Discriminating Clear-Sky from Cloud with MODIS: Algorithm Theoretical Basis Document (MOD35).* Algorithm Theoretical Basis Document ATBD-MOD-06, NASA Goddard Space Flight Center, 125 pp.

Barkstrom, B., 1984: The Earth Radiation Budget Experiment (ERBE). *Bull. Amer. Meteor. Soc.*, **65**:1170–1185.

Colbo, K. and R. A. Weller, 2009: Accuracy of the IMET sensor package in the subtropics. *J. Atmos. Oceanic Technol.*, **26**:1867–1890.

Gerber, H., G. Frick, S. P. Malinowski, J-L. Brenguier, and F. Burnet, 2005: Holes and entrainment in stratocumulus. *J. Atmos. Sci.*, **62**:443–459.

Haynes , J. M., T. S. L'Ecuyer, G. L. Stephens, S. D. Miller, C. Mitrescu, N. B. Wood, and S. Tanelli, 2009: Rainfall retrieval over the ocean with spaceborne W‐band radar, *J. Geophys. Res.*, **114**, D00A22, doi:10.1029/2008JD009973.

IPCC, 2007: *Climate Change 2007: The Physical Science Basis. Contribution of Working Group I to the Fourth Assessment Report of the Intergovernmental Panel on Climate Change* [Solomon, S., D. Qin, M. Manning, Z. Chen, M. Marquis, K.B. Averyt, M.Tignor and H.L. Miller (eds.)]. Cambridge University Press, Cambridge, United Kingdom and New York, NY, USA.

King, M. D., S.-C. Tsay, S. E. Platnick, M. Wang, and K.-N. Liou, 1997: *Cloud Retrieval Algorithms for MODIS: Optical Thickness, Effective Particle Radius, and Thermodynamic Phase: MOD06 – Cloud Product*. MODIS Algorithm Theoretical Basis Document No. ATBD-MOD-05, Version 5.

Klein, S. A. and D. L. Hartmann, 1993: The seasonal cycle of low stratiform clouds. *J. Climate*, **6**:1587–1606.

L'Ecuyer, T., 2007: Level 2 Fluxes and Heating Rates Product Process Description and Interface Control Document Version 5.1

L'Ecuyer, T. S. and G. L. Stephens. 2002. An estimation-based precipitation retrieval algorithm for attenuating radars. *J. Appl. Meteor.*, **41**:272–285.

Leon , D. C., Z. Wang, and D. Liu, 2008: Climatology of drizzle in marine boundary layer clouds based on 1 year of data from CloudSat and Cloud   Aerosol Lidar and Infrared Pathfinder Satellite Observations (CALIPSO), *J. Geophys. Res.*, **113**, D00A14, doi:10.1029/2008JD009835.

Ma, C.-C., C. R. Mechoso, A. W. Robertson, and A. Arakawa, 1996: Peruvian stratus clouds and the tropical Pacific circulation: A coupled ocean–atmosphere GCM study. *J. Climate*, **9,** 1635–1645.

Mace, G., 2007: Level 2 Radar-Lidar GEOPROF Product Process Description and Interface Control Document Version 1.0

Marshall, J. S. and W. M. Palmer, 1948: The distribution of raindrops with size. *J. Meteor.*, **5**:165–166.

Menzel, W. P., and K. Strabala, 1997: *Cloud Top Properties and Cloud Phase: Algorithm Theoretical Basis Document*. ATBD-MOD-04, NASA Goddard Space Flight Center, 55 pp.

Petters , M. D., J. R. Snider, B. Stevens, G. Vali, I. Faloona, and L. M. Russell, 2006: Accumulation mode aerosol, pockets of open cells, and particle nucleation in the

remote subtropical Pacific marine boundary layer, *J. Geophys. Res.*, **111**, D02206, doi:10.1029/2004JD005694.

Randall, D. A., J. A. Coakley, D. H. Lenschow, C. W. Fairall, and R. A. Kropfli, 1984: Outlook for research on subtropical marine stratiform clouds. *Bull. Amer. Meteor. Soc.*, **65**:1290–1301.

Sharon, T. M., B. A. Albrecht, H. H. Jonsson, P. Minnis, M. M. Khaiyer, T. M. van Reken, J. Seinfeld, and R. Flagan, 2006: Aerosol and cloud microphysical characteristics of rifts and gradients in maritime stratocumulus clouds. *J. Atmos. Sci.*, **63**:983–997.

Slingo, A., 1990: Sensitivity of earth's radiation budget to changes in low clouds. *Nature*, **343**:49–51.

Stevens, B., W. R. Cotton, G. Feingold, and C-H. Moeng, 1998: Large-eddy simulations of strongly precipitating, shallow, stratocumulus-topped boundary layers. *J. Atmos. Sci.*, **55**:3616–3638.

Stevens, B., G. Vali, K. Comstock, R. Wood, M. C. van Zanten, P. H. Austin, C. S. Bretherton, and D. H. Lenschow, 2005: Pockets of open cells and drizzle in marine stratocumulus. *Bull. Amer. Meteor. Soc.*, **86**:51–57.

Twohy , C. H., M. D. Petters, J. R. Snider, B. Stevens, W. Tahnk, M. Wetzel, L. Russell, and F. Burnet, 2005: Evaluation of the aerosol indirect effect in marine stratocumulus clouds: Droplet number, size, liquid water path, and radiative impact, *J. Geophys. Res.*, **110**, D08203, doi:10.1029/2004JD005116.

vanZanten, M.C., and B. Stevens, 2005: Observations of the Structure of Heavily Precipitating Marine Stratocumulus. *J. Atmos. Sci.*, **62**, 4327–4342.

vanZanten, M. C., B. Stevens, G. Vali, and D. Lenschow, 2005: Observations of drizzle in nocturnal marine stratocumulus. *J. Atmos. Sci.*, **62**:88–106.

Warren, S.G., C.J. Hahn, J. London, R.M. Chervin and R.L. Jenne, 1986: Global distribution of total cloud cover and cloud type amounts over land. NCAR Tech. Note, NCAR/TN-273+STR, 29 pp. + 200 maps.

Warren, S.G., C.J. Hahn, J. London, R.M. Chervin and R.L. Jenne, 1988: Global distribution of total cloud cover and cloud type amounts over the ocean. NCAR Tech. Note, NCAR/TN-317+STR, 41 pp. + 170 maps.

Wood, R., 2005a: Drizzle in stratiform boundary layer clouds. Part I: Vertical and horizontal structure. *J. Atmos. Sci.*, **62**:3011–3033.

Wood, R., 2005b: Drizzle in stratiform boundary layer clouds. Part II: Microphysical aspects. *J. Atmos. Sci.*, **62**:3034–3050.

Wyngaard, J. C., and C.-H. Moeng, 1990: A global survey of PBL models used within GCMs. *Proceedings of a PBL Model Evaluation Workshop: European Centre for Medium-Range Forecasts,* P. Taylor and J. C. Wyngaard, Eds., World Climate Research Program Series 42, WMO/TD 378, 38–59.

Zhang, Y., B. Stevens, and M. Ghil, 2005: On the diurnal cycle and susceptibility to aerosol concentrations in a stratocumulus-topped mixed layer. *Quart. J. Roy. Meteor. Soc.*, **131**:1567–1583.